University of Alberta

EXPLOSIVE PLASMA INSTABILITIES IN THE NEAR-EARTH MAGNETOTAIL: A
GEOMETRICAL TREATMENT

by

©

Peter Dobias

A thesis submitted to the Faculty of Graduate Studies and Research in partial fulfillment
of the requirements for the degree of **Doctor of Philosophy.**

Department of Physics

Edmonton, Alberta
Fall 2002

0-612-81182-4

Canada

University of Alberta

Library Release Form

Name of Author: Peter Dobias

Title of Thesis: Explosive Plasma Instabilities in the Near-Earth Magnetotail: A Geometrical Treatment

Degree: Doctor of Philosophy

Year this Degree Granted: 2002

Permission is hereby granted to the University of Alberta Library to reproduce single copies of this thesis and to lend or sell such copies for private, scholarly or scientific research purposes only.

The author reserves all other publication and other rights in association with the copyright in the thesis, and except as hereinbefore provided, neither the thesis nor any substantial portion thereof may be printed or otherwise reproduced in any material form whatever without the author's prior written permission.

Peter Dobias

Peter Dobias
University of Alberta
Edmonton, AB
Canada, T6G 2J1
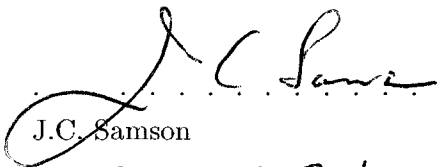
Date: *Aug 30, 2002*
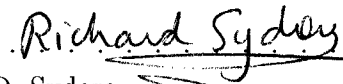
It is the glory of God to conceal a matter,
But the glory of kings is to search out a matter...(Prov. 25:2)

University of Alberta
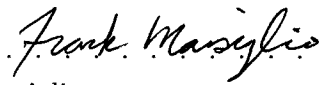
Faculty of Graduate Studies and Research

The undersigned certify that they have read, and recommend to the Faculty of Graduate Studies and Research for acceptance, a thesis entitled **Explosive Plasma Instabilities in the Near-Earth Magnetotail: A Geometrical Treatment** submitted by Peter Dobias in partial fulfillment of the requirements for the degree of **Doctor of Philosophy**

J.C. Samson

R.D. Sydora

R. Marchand

F. Marsiglio

R. Fedosejevs

P. Guzdar

Date: Aug 26, 2002

To the Glory of God.

Abstract

Explosive instabilities in plasmas are one of the most frequent, yet least understood phenomena in physics. In this thesis we present a method of investigating non-linear (explosive) plasma instabilities based on the combination of a variational approach with differential geometry. This method makes it possible to resolve questions about non-linear stability without solving the full non-linear dynamical equations. We demonstrate this method for the case of ideal magnetohydrodynamics (MHD) which is an excellent approximation of plasma behavior for many physical systems. At the end we apply this method to two examples of plasma instability investigation, in rectilinear, and in a curved magnetic field topology.

In the first example, plasma in a box, we know apriori that the system must be stable in the absence of gravity, since there is no source of free energy that could drive the instability. This simple example illustrates the simplicity of the method we developed.

The second example deals with plasma in a curvilinear, stretched magnetic field topology. Since the stretching of the field lines provides a source of free energy, it is possible for an instability to develop. In the case we present we demonstrate that initial linear instability evolves into an explosive behavior on a very short time scale. This result is consistent with the results obtained from global MHD modeling.

Possible applications for this method are space weather prediction, and the improvement in our understanding of explosive processes in magnetically confined plasmas.

Acknowledgements

I want to thank my family, especially my wife Zuzana, for their patience and for the overwhelming support they gave me during my research work. I'm also very thankful to my supervisor, Dr. John Samson, for introducing me to this challenging research area and for all help and encouragement he gave me. Special thanks go to Dr. Vladimir Tikhonchuk for many fruitful discussions that helped me in building this model and to Peter Damiano whose suggestions helped me to speed up the code development process. Finally I'm also grateful to Dr. Igor Voronkov for providing me with the results of his ADI code and for valuable discussions on plasma instabilities.

Contents

List of Figures

Chapter 1

Introduction

One of the most challenging topics in the physics of plasmas is the understanding of non-linear instabilities responsible for rapid energy redistribution in plasmas. This is especially true in magnetically confined plasmas that are found in both space and laboratory plasmas. Examples of nonlinear instabilities that have explosive behavior can be found in both, space plasmas (solar flares, Fig. 1.1, magnetic substorms, Fig. 1.2, 1.5) and in laboratory plasmas (core crashes in TOKAMAKs). In this context we use the term "explosive" for instabilities that have Alfvénic time scales. In the Earth's magnetosphere the instability develops faster than the information propagates via shear Alfvén waves to the ionosphere. Despite the prevalence of these instabilities, our understanding of the physics of these processes is very limited. This situation is partially due to limited experimental data, since the temporal scale of the dynamics of the instabilities is often beyond the time resolution of present observations, particularly in space-based experiments. Furthermore, the equations describing the plasma processes are often very complicated and do not allow a simple analysis. However, the importance of understanding plasma behavior during explosive instabilities, especially our ability to predict these explosions, is increasing due to the technological use of near-earth space and the demand for new energy sources through magnetic confinement fusion. For instance, core crashes are one of the main obstacles in performing controlled thermo-nuclear fusion, which would provide an abundant source of energy for society. Magnetospheric substorms can have damaging effects on many man-made devices (satellites) in space (Fig. 1.3), and they can also negatively influence ground based telecommunication and broadcast networks, including malfunctioning of GPS systems and damage to power lines and pipeline systems. Fig. 1.4 shows a map of the power outages in North America caused by the magnetic storm in March 1989.

A most promising method for the investigation of nonlinear and explosive plasma insta-

bilities appears to be a variational approach [*Ilginois and Pastukhov*, 2000]. In this work we present a new method for the investigation of non-linear plasma instabilities. This method combines a variational and perturbation approach. In the calculations we employ differential geometry which simplifies the algebra significantly, and provides us with compact results that can be readily used for investigation of various plasma configurations. We will illustrate the efficiency of our method by looking at instabilities in the near Earth magnetotail during the explosive phases of auroral and magnetospheric substorms.

Figure 1.1: Solar flares are one of the most violent events in solar system. (Photograph courtesy NASA.)
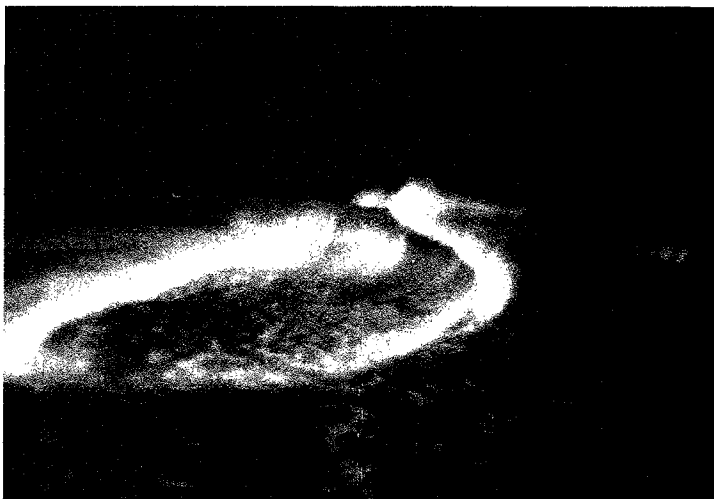
Figure 1.2: A view of aurora australis - southern lights from the Space Shuttle Discovery. (Photograph courtesy of NASA.)
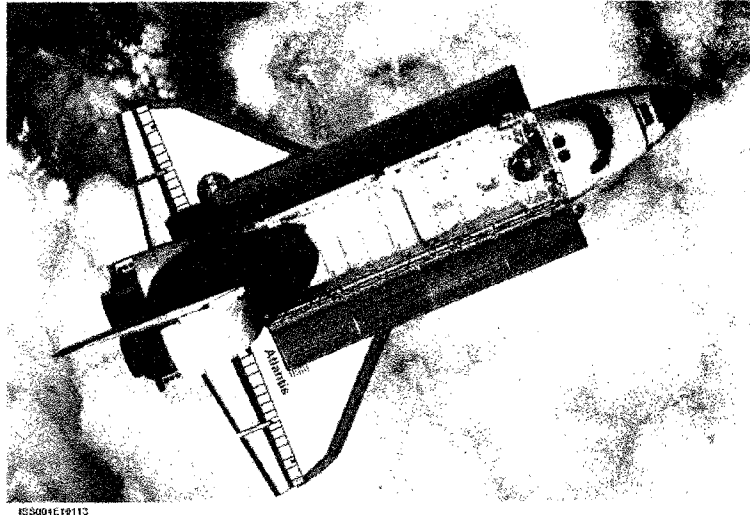
Figure 1.3: Space Shuttle Atlantis. Satellites and shuttles can be seriously damaged by the electro-magnetic disturbances due to explosive instabilities in magnetosphere. (Photograph courtesy NASA.)
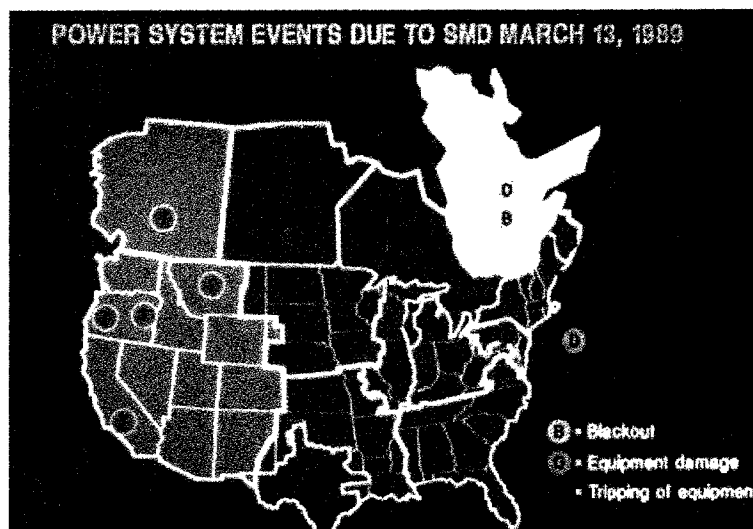
Figure 1.4: Map of the power outages in North America due to the magnetic storm in March 1989. (Map courtesy EPRI.)

3

1.1 Modeling of Plasma Instabilities

Modeling of the instabilities in magnetically confined plasmas brings many challenges. No matter what description is used, whether kinetic or fluid, the description always involves sets of coupled non-linear equations. In the case of small perturbations and reasonably slow processes, these equations can usually be linearized. Nevertheless, even the linear equations are rather complicated and additional assumptions, as are for instance special geometry or harmonic dependence of certain component, are often needed to solve them. There is, however, rather good understanding of many processes that can be described within a linear theory. On the other hand, if the processes involved in the phenomena of interest happen too rapidly or involve large gradients of plasma parameters, non-linear behavior is often important, and cannot be easily ignored. Then it is necessary to use some restrictions on the system that might be physically justifiable to convert the problem into a form for which solution might be known. This is called the method of analogs and is based on the fact that mathematically equivalent equations will have the same solutions no matter what physical system they describe. For detailed treatment of this method see e.g. the excellent work by *Feynman et. al.* [1977]. Many times, as we shall show in this thesis, a completely new mathematical approach might be required. But even then the problem may be too complicated to be fully resolved, and computational models are needed.

The understanding of the dynamics of explosive instabilities is clearly of the utmost importance in many areas of plasma physics. Even an ability to predict, with high accuracy, when and where the instability will start would be a big step forward in our understanding of the plasma dynamics, and would open new opportunities for many applications in space and laboratory plasmas.

1.2 Core Crashes in Tokamaks

As an example of explosive, non-linear instabilities core-crash events in TOKAMAKs are an important problem in the physics of fusion. They are characterized by [*Itoh et al.*, 1998]

- sudden onset of symmetry breaking perturbations

- bursts of energy, momentum and particles across magnetic surfaces

- avalanches of collapse events (A disruption starts in a localized area, but it propagates to surrounding areas and disrupts them [*Cowley and Artun*, 1997]. These areas can then become the source of new disruptions.)

4

- unpredictability

These events cannot be described within linear theory, although a lot of work, including the introduction of various dissipation mechanisms has been done in attempts to match observations and theory [*Itoh et al.*, 1998]. The crash events usually start with the sudden growth of one of the plasma modes, which then causes disruption of the whole system. Time-scales of these processes are extremely short, much shorter than the collision times in the plasma. Sometimes the system recovers after the crash and then the crash can repeat itself. At other times the disruption is on a global scale, and the system does not recover.

Since the crash phenomena are limiting the possibilities of the use of toroidal plasmas, they are one of the essential problems of magnetic confinement studies. Due to the rapid time scales and non-local disruptions of the ambient plasmas, the full description of these processes is one of the great challenges for the physics of non-equilibrium plasma [*Itoh et al.*, 1998].

1.3 Magnetospheric Substorms

Although the applicability of the physics involved in the description of the explosive instabilities is very wide [*Ortolani and Schnack*, 1993], our focus is primarily on the understanding of magnetospheric substorms (see e.g [*Rostoker et. al.*, 1980]). The situation in space plasmas is slightly more complicated than in laboratory plasmas, since the system is not closed and external factors contribute to the dynamics of the system. However, we believe that the fundamental nature of the instabilities in the magnetosphere is the same as in laboratory plasmas. In this work we are not trying to develop a full dynamic description of the explosive instability in the magnetosphere. We limit ourselves to the development of a model that allows the identification of explosively unstable plasma configurations in the magnetosphere, and thus when and where we can expect the onset of substorm intensification and expansive phase.

The term *magnetospheric substorm* describes a process of storage of solar wind energy in the Earth's magnetosphere, particularly the magnetotail, and then the sudden release of this energy causing auroral and magnetic disturbances. These disturbances are responsible for the brightening of auroral arcs (Fig. 1.5). Some auroral arcs are thought to be produced by ultra low frequency (1-4 mHz) shear Alfvén modes that lead to explosive instabilities in the night-side magnetosphere [*Samson et. al.*, 1992]. An example of the near Earth magnetotail configuration just prior to the substorm is shown in Fig. 1.6. The topology is "stretched"

5

Figure 1.5: A photograph of auroral arcs (Photograph courtesy of NASA).

beyond the dipolar configuration indicating a storage of energy. This "stretched" field topology plays an important role in the onset of explosive, nonlinear MHD instabilities.

The magnetic substorm has five phases:

i. Growth Phase (duration 10s of minutes)

ii. Precursor Phase (duration minutes)

iii. Intensification Phase (duration 10s of seconds)

iv. Expansion Phase (duration 10s to 100s of seconds)

v. Recovery (lobe flux reconnection) (duration minutes)

During the growth phase, the interaction between solar wind and magnetosphere leads to slow adiabatic storage of energy in the magnetotail with the stretching of tail field lines and an increase in the open flux connected to the interplanetary magnetic field. Strong plasma pressure gradients develop near the Earthward edge of the plasma sheet. In line with this slow growth, the configuration of the magnetotail remains linearly or near linearly stable.

In the precursor phase an auroral arc forms on field lines threading the Earthward edge of the plasma sheet. This arc then forms azimuthally periodic vortex structures with an azimuthal wavelength of about 100-200 km. Ballooning modes might play an important role in the formation of these vortices [Voronkov et. al., 1997]. This instability can trigger

6

the substorm intensification, but does not always do so. When the substorm intensification and expansive phase do not occur, then we can refer to the process as a pseudo breakup.

During the intensification phase the auroral arc brightens and develops large scale vortex structures, followed by the poleward expansion of the auroral surge, and enhanced electrojets. The time scales (10s of seconds) of the surge formation and explosive cross tail current growth are comparable to Alfvénic time scales in the near Earth magnetotail, indicating an explosive and nonlinear instability, possibly ballooning. This process is likely to be connected with the explosive growth phase in the near Earth cross tail current [*Ohtani et al.*, 1992]. Another possible mechanism leading to this nonlinear ballooning phase is the detonation model ([*Cowley and Artun*, 1997] and [*Hurricane et al.*, 1997]). The detonation model does not require a precursor mode to push the system into a nonlinearly unstable regime.

In the expansion stage the energy accumulated in the tail is released. Ballooning leads to a highly stretched tail magnetic field topology near the Earth, with enhanced cross tail currents. The increased effective Hall conductivity of the plasma leads to a hybrid ballooning- tearing mode or a region of localized reconnection, and the beginning of the dipolarization of magnetic field lines in the near Earth region.

The time scales of the intensification and expansion phases are very short (Alfvenic time scale) [*Friedrich et al.*, 2001]. This suggests that the plasma dynamics involved in these processes is explosively non-linear. The last stage of the substorm is the recovery (lobe flux reconnection) phase. It begins when the region of localized tearing or reconnection reaches lobe field lines. Then closure of open field flux begins. This phase is compatible with the near Earth neutral line (NENL) model of substorm expansion [*Baker et al.*, 1996]. Optical data indicate that this might occur at about 15-30 Earth radii down the magnetotail. The recovery phase can sometimes overlap with another growth phase.

Optical measurements of auroral emissions associated with a magnetospheric substorm are shown in Fig. 1.7. The growth phase lasts from 03:00 to just after 04:30. The equator-ward motion of H-β emission (486.1 nm) is due to equator-ward motion of energetic H$^+$ precipitation due to energy storage and stretching of field lines in the near Earth magnetotail. The onset of the intensification and expansive phase is clearly visible in the middle part of the figure, occurring at about 04:35. Here the explosive onset and release of energy is associated with the dipolarization of near Earth field lines, leading to poleward motion of energetic H$^+$ precipitation.

In terms of space weather prediction one of the great challenges is to decide when and

where the substorm intensification will occur. This ability would give us an opportunity to possibly protect the most sensitive space based and ground based systems from the adverse effects due to the electro-magnetic perturbations and energetic particles. To do that, it is important to be able to classify possibly unstable configurations of the magnetosphere. Although linear stability criteria can be defined for general curvilinear coordinates [*Liu*, 1997], we have very limited understanding of the non-linear instabilities which are responsible for substorm onset. We shall address this issue in this thesis.

One of the possible applications of the method we present in this thesis can be testing of data (or simulation) based equilibrium models for potentially explosively unstable regions. Ideally, these tests could be incorporated into global MHD models and serve for space weather prediction.

8
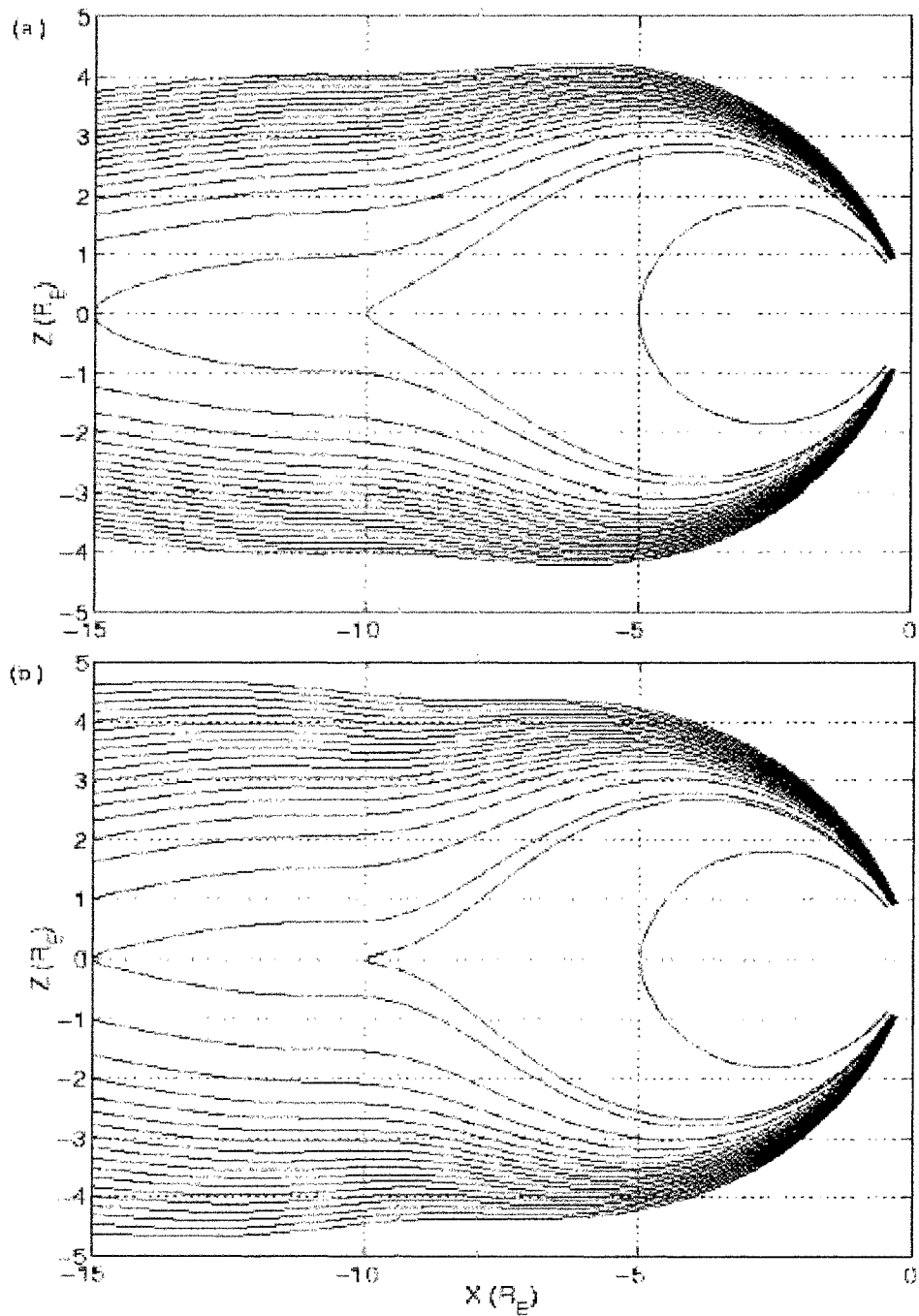
Figure 1.6: Magnetospheric configuration prior to the substorm onset phase as constructed from optical data constraints [*Wanliss et al.*, 2000]. Figures a) and b) show magnetotail at two different times during the growth phase of the same event.

9
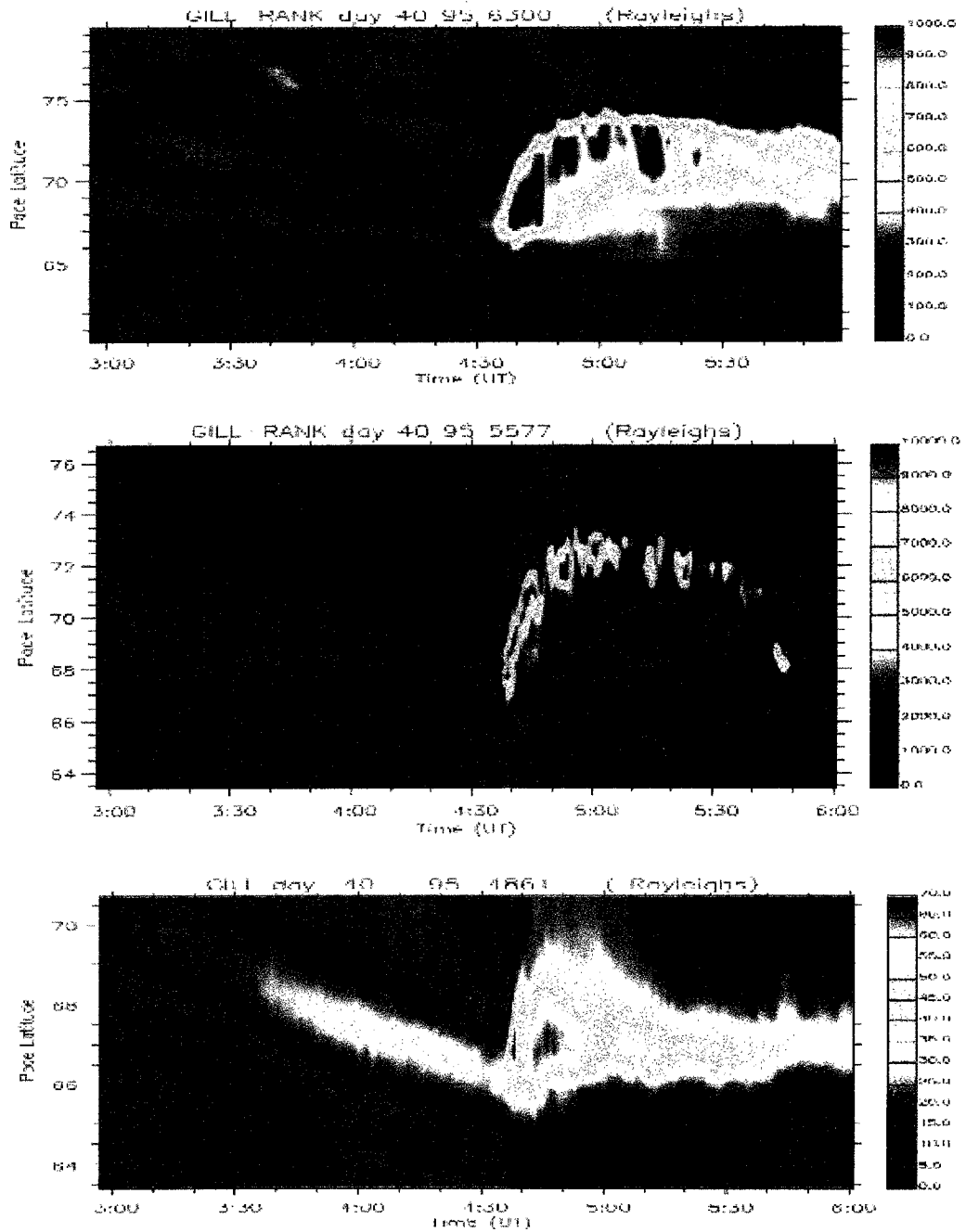
Figure 1.7: Example of the substorm as seen in CANOPUS data. This event happened on 09/02/1995. A long period of growth phase is followed by an extremely fast disruption. [*Wanliss et al.*, 2000]

10

1.4 Outline of the Method

In this thesis we are not attempting to resolve the full non-linear dynamics of the substorm intensification and expansion phase. This full description will have to include a kinetic description since the timescales in the magnetotail (the region of destabilization) are on the order of, or shorter than the ion gyroperiod (10s of seconds). Furthermore, the full dynamics presents an extremely complicated problem, possibly ranking as a "grand challenge problem" in plasma physics. Instead, we present a method of investigating the conditions for the onset of explosive instabilities in an arbitrary magnetic field configuration, without the need to solve the non-linear equations. It is based on a method using analogies between different physical systems obeying similar equations, and therefore exhibiting qualitatively similar behavior [*Feynman et al.*, 1977]. This method provide a means of bypassing the complicated calculations contained in the full dynamics.

Our method uses a variational approach which seems to be very effective in the identification of nonlinearly unstable plasma configurations [*Pfirsch and Sudan*, 1993; *Ilginois and Pastukhov*, 2000]. Also, the use of differential geometry, namely use of a component formalism and transformation rules, as a mathematical tool greatly simplifies the otherwise extremely complicated expressions found by using vector analysis. This combination of a variational and geometrical approach leads to a much more tractible model for the analysis of non-linear instabilities particularly in magnetospheric plasmas.

Key points of this method are:

- **The use of a Lagrangian of the system** - the Lagrangian is a scalar quantity and therefore it has the same form in any coordinate system.

- **Analogy with mechanics** - here we utilize the fact that equivalent equations have equivalent solutions. As an example consider the equation $\ddot{a} = -a$. This equation yields a solution $a = a_0 \exp(it)$ with no regard for the meaning of the symbol a. It can be a displacement in mechanics or an electric field. Usually mechanical systems are more intuitive and easier to understand than the dynamics of a magnetized charged fluid. Also, it is generally much easier to find solutions for mechanical systems than for plasmas, and by finding similar mathematical description for plasma and for mechanical system, we can describe the qualitative behavior of the plasma using the behavior of the mechanical system that we are often able to resolve.

11

- **Perturbation is treated as a coordinate change** - this is the method commonly used in the theory of elasticity. It eliminates the need for the use of additional equations connecting perturbations in different physical quantities. Instead, we can easily obtain expressions for perturbed quantities in terms of coordinate shifts from conservation laws (constraints in the Lagrangian).

- **The use of differential geometry.** This includes the use of a component formalism instead of a traditional vector analysis, and also the use of transformation rules for the coordinates. The component formalism significantly simplifies notation, plus it makes possible the derivation in an arbitrary geometry, so the results are equally valid for a box, for stretched field lines in the magnetosphere and for the toroidal fields in TOKAMAKs. The use of the transformation rules that have a simple form in terms of geometry helps us to limit requirements for additional physical assumptions. For more details on approaches using differential geometry see e.g. [*Flanders*, 1963; *Schutz*, 1980].

To summarize, our method can be outlined in following steps:

i. Define Lagrangian of the system.

ii. Calculate perturbation up to the third order in plasma displacement.

iii. Derive linear equation of motion.

iv. Define initial parameters for the plasma.

v. Calculate plasma displacement in linear approximation.

vi. Calculate the second and the third order potential energies using results from the linear model.

vii. Identify possible unstable behavior.

We demonstrate the application of this geometrical method using ideal magnetohydrodynamics (MHD). This approximation is rich enough to contain non-trivial physics, but still simple enough to demonstrate the beauty of this method, without getting lost in complicated algebra. Then we investigate the non-linear stability of several different plasma configurations within the framework of ideal MHD in order to demonstrate the use of this method on real problems, including the magnetospheric substorm.

12

Chapter 2

Lagrangian Formulation of Non-linear Stability Criteria: Theory

2.1 Situation in Classical Mechanics

The behavior of an object in classical mechanics is fully defined by specifying forces $F(x,v)$ acting on the object and the position x and velocity v of the object at some time. For a more detailed treatment of classical mechanics see e.g. [*Landau and Lifshitz*, 1976]. In many situations it is reasonable to assume that the force is a function of coordinates only ($F(x,v) \equiv F(x)$). Then the force can be alternatively described by a potential $U(x)$ such that $F(x,v) = -dU(x,v)/dx$. The system can be described by the Lagrangian

$$L(x,v) = m\frac{1}{2}v^2 - U(x),\tag{2.1}$$

where m is mass of the object, and we assume kinetic energy in the form $T = mv^2/2$. Here we ignore for instance systems including a Lorentz force. The potential $U(x)$ can be expanded around some arbitrary point x_0 as

$$U(x) \;=\; U(x_0) + \frac{dU(x_0)}{dx}(x - x_0) + \frac{1}{2}\frac{d^2U(x_0)}{dx^2}(x - x_0)^2 + $$
$$+ \; \frac{1}{6}\frac{d^3U(x_0)}{dx^3}(x - x_0)^3 + \mathrm{O}\Big((x - x_0)^4\Big).\tag{2.2}$$

Since a constant potential has no effect on the dynamics of the system, we can assume it is equal to zero. Also, we can choose a coordinate system such that $x_0 = 0$. Then the potential (2.2) can be written as

$$U(x) = \gamma x + \frac{1}{2}\alpha x^2 + \frac{1}{3}\beta x^3 + \mathrm{O}(x^4),\tag{2.3}$$

13

where α, β and γ are constants that correspond to the coefficients of the Taylor expansion (2.2), and the Lagrangian (2.1) can be written in the form

$$L(x, v) = m\frac{1}{2}v^2 - \gamma x - \frac{1}{2}\alpha x^2 - \frac{1}{3}\beta x^3 + O(x^4), \tag{2.4}$$

corresponding to the equation of motion in the form

$$m\frac{dv}{dt} = -\gamma - \alpha x - \beta x^2 + O(x^3). \tag{2.5}$$

If $\alpha = \beta = 0$ this equation describes uniform acceleration $a = -\gamma$. If $\gamma = \beta = 0$ this equation takes the form

$$m\frac{dv}{dt} = -\alpha x, \tag{2.6}$$

with the solution

$$x = x_0 \exp(\pm i\sqrt{\alpha/m}\, t) \tag{2.7}$$

which describes either a harmonic oscillator or an exponentially decaying or growing system, depending on the sign of α (wave propagation and damped and growing modes in plasmas).

If $\alpha = \gamma = 0$ the system is described by the equation

$$m\frac{dv}{dt} = -\beta x^2, \tag{2.8}$$

which has a singular solution

$$x = \frac{-6m}{\beta(t - t_0)^2}. \tag{2.9}$$

Since this solution is singular, from a certain point it must grow faster than exponential. Similar solutions for plasma configurations correspond to explosive instabilities in plasmas.

Behavior due to the second and the third order terms can also be understood qualitatively from Figure (2.1). In the case of a quadratic dependence of the potential energy, a ball is either in a valley where it will roll from one side to the other, which corresponds to a harmonic oscillator, or it is on a hill, where it will eventually roll down. In the case of a cubic dependence there is no well, the ball has a stationary point at $x = 0$, but once it starts moving, it will always end up rolling down the hill. If the potential energy is a mix of comparable second and third order contributions, the ball can either roll down the hill, or can stay trapped in the well. It is necessary to solve the equation of motion for each specific situation. However, if the initial push is strong enough, or the system is not closed and can experience additional smaller pushes, eventually there is a great chance that the ball will end up rolling down the hill.

14
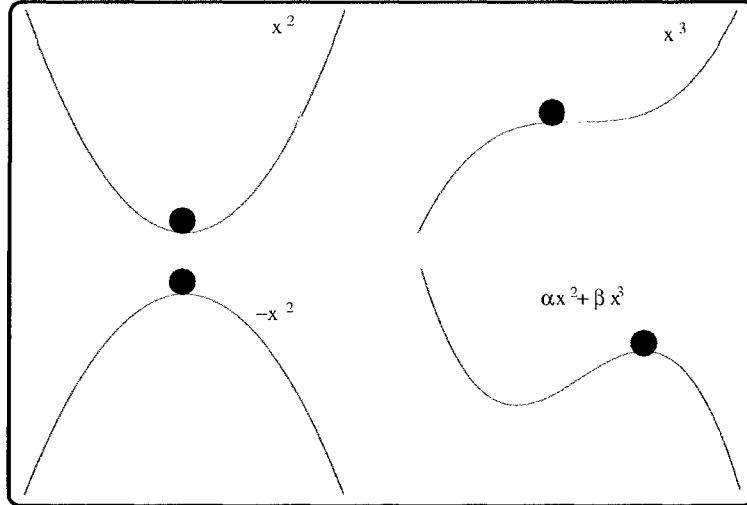
Figure 2.1: Qualitative sketch of the second and the third order potential energy. Pure second order allows either stable or unstable solutions (the ball is either on the top of a hill or in a well). Pure third order energy always lead to a singular solution (no matter what the ball does, it will eventually roll downhill). Mixed energy requires full information about the dynamics to decide the motion.

So far we dealt only with the one dimensional problem. The situation in more dimensions will be similar, but richer. The motion can be stable in one direction and unstable in the other direction, or can be linearly unstable in one direction and explosive in the other direction. However, the general characteristics remain the same (Figure 2.2).

2.2 Plasma Instabilities

2.2.1 General Methodology

As we mentioned, our method provides us with a tool for the investigation of plasma susceptibility to explosive instabilities. This method works for any model describing plasmas, for which a Lagrangian can be defined. Also, we show that the use of a component formalism makes this method more practical than a vector formalism, since the amount of algebra is significantly reduced compared to traditional approaches, and also the results are in a very efficient form which makes further calculations much easier.

The form of the geometrical approach is, in fact, very simple. In analogy with the mechanical systems discussed in the previous section, we assume that if in some local domain in the plasma the third order potential energy dominates over the second order, the plasma in this domain is explosively unstable. Once the instability starts, if there is enough free energy in the system, it can eventually also perturb the surrounding plasma that was

15
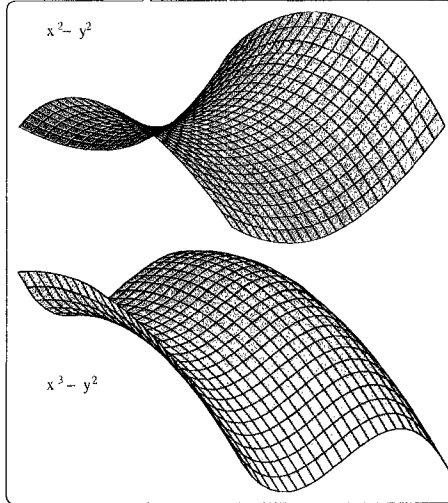
Figure 2.2: Qualitative sketch of the second and third order potential energy in 2-dimensions. This situation is similar to the 1-dimensional case, but more possibilities exist. A situation stable in one direction and unstable in the other direction, and a situation linearly unstable in one direction and explosive in the other one is shown.

originally metastable, leading to further growth of the unstable region [*Hurricane et al.*, 1999]. Also, if the second and the third order potential energies are comparable, we cannot predict the behavior of the plasma without resolving the full dynamics. We can, however, expect that due to an additional push, from the solar wind or field-line resonances (FLR) in the magnetosphere (see [*Samson et. al.*, 1992], for instance), an instability can start. Also, in linearly unstable regions with comparable second and third order energies, an originally linear instability can trigger an explosive behavior. If the second order potential energy dominates everywhere, the system is well described by the linear equations and we do not expect an explosive instability to occur.

The method we developed consists of four main steps

- Define the Lagrangian of the system (MHD, two-fluid, kinetic) and all the additional constraints. These constraints are necessary, otherwise the Lagrangian would describe only a trivial solution. Also, these constraints define transformation properties of the physical quantities involved.

- Calculate the perturbed Lagrangian up to the third order in the plasma displacement $\xi(x, t)$ which is defined as the coordinate shift

$$\hat{x} = x + \xi(t, x),$$ (2.10)

where the displacement ξ is a function of the original coordinates x, and time t. Also,

16

we assume that the displacement ξ is small enough so that we can use it as the ordering quantity for a perturbation treatment of the plasma. Here the use of the component formalism and of the apparatus of differential geometry helps to reduce significantly the amount of algebra needed as compared to traditional vector approaches, used for instance by *Pfirsch and Sudan* [1993]. Also the results are in very compact form and are ready for further calculations.

- The first order term yields the equilibrium condition for the unperturbed quantities

$$L^{(1)} \equiv \int dV \mathcal{L}^{(1)} = 0. \tag{2.11}$$

The condition for the second order term

$$L^{(2)} \equiv \int dV \mathcal{L}^{(2)} = 0 \tag{2.12}$$

yields the linear equation of motion for the plasma within the chosen model. This linear equation will have the form of a wave equation, and it is the most general linear equation that can be derived for the plasma. Applying additional assumptions to this equation makes it possible to obtain many classical results, as will be shown in the next part. Solving this linear equation for a chosen plasma configuration yields the class of possible displacements as a function of the coordinates. Here we assume that the linear solution is a reasonable approximation for the plasma displacement, since we are not trying to describe the actual dynamics of the non-linear stage (we only want to be able to predict possible instability onset). For instance we can expect that the growth phase of the magnetospheric substorm is well described by the linear equations all the way until the onset of the substorm intensification and expansive phase.

- The last step is to calculate maps of both the second and the third order potential energy densities ($W^{(2)}$ and $W^{(3)}$). Then the regions where these energy densities are comparable, or the third order dominates must be identified. These regions are possible sources of explosive instability in the plasma. After the unstable domains with $W^{(2)} \ll W^{(3)}$ are determined, we can assume that explosive behavior starts. Also, in the areas with $W^{(2)} \sim W^{(3)}$ that are linearly unstable, we can assume that the linear instability triggers explosive behavior which will eventually dominate.

By following this procedure we can resolve the question of the possible beginning of the explosive instability by solving the equations describing the linear dynamics of the system.

17

2.2.2 The Fourth Order Term

The question can be raised about the influence of the fourth order term in the Lagrangian on the dynamics of the instability. We will show that this term does not influence the dynamics of the system at the point of the explosive instability onset. This term can affect the nonlinear stage of the dynamics, but this phase is beyond the objective of our model. We will treat the problem of the fourth order term in two steps. First, we estimate the magnitude of the fourth order coefficient and compare it to the lower orders. Then we will show that the general requirement of the perturbation calculations requires that the fourth order term be initially much smaller than the second and third order terms.

To estimate the value of the fourth order coefficient, we must return to the transformation properties of the ambient physical quantities in terms of the plasma displacement $\boldsymbol{\xi}$. A general quantity X transforms as

$$\hat{X} = \bar{T}(\boldsymbol{\xi}) \cdot X, \tag{2.13}$$

where is $\bar{T}$ is a matrix transforming quantity X. In other words, the dependence on the plasma displacement is limited to the transformation matrix, and therefore the expansion must be limited to this matrix as well. Also, the expansion coefficients must contain unperturbed physical quantities as were contained in the original Lagrangian to preserve dimensions of the expansion terms. This defines the scale of the expansion terms, and the differences in their values can originate only from the expansion of the matrix $\bar{T}$.

Since the matrix $\bar{T}$ is connected to the coordinate change (2.10), it must contain the Jacobian matrix $J_j^i \equiv (d\hat{x}^i/dx^j)$ and the Jacobian $J = \det(J_j^i)$ of the transformation (2.10). Since the transformation (2.10) is linear in the displacement, the Jacobian matrix must be of the form of a power function in the plasma displacement ξ. Therefore the transformation matrix $\bar{T}$ will have the shape of a rational function. The coefficients in the expansion will be either approximately the same for all the orders, or, more likely, they will have decreasing values such that the n-th term will be a factor $1/n$ smaller than the $(n-1)$-st term. This means that the fourth order coefficient will be no greater than the lower order coefficients, and likely will be smaller by a factor of four.

For the Taylor expansion to converge we must require the gradients of the plasma displacement (2.10) $\xi^i_{,j} \ll 1$ [$\check{S}vec\ et\ al$, 1987]. Otherwise they would not be suitable as the ordering quantity. Therefore, initially the ordering of the terms

$$L^{(0)}(1) \gg L^{(1)}(\boldsymbol{\xi}) \gg L^{(2)}(\boldsymbol{\xi}^2) \gg L^{(3)}(\boldsymbol{\xi}^3) \gg L^{(4)}(\boldsymbol{\xi}^4) \gg ... \tag{2.14}$$

18

must hold.

Naturally, the dynamic behavior of the system can be such that the gradients of plasma displacement ξ^i_j would grow and eventually the ordering (2.14) will be violated. When this happens, the higher order terms are becoming important. At this point the linear approximation ceases to be valid, and we are looking at the onset of non-linear behavior. However, continuity of the expanded Lagrangian requires that the higher order terms become important with a time sequence corresponding to their order. Therefore, at least for a limited time, the third order term will govern the dynamics of the system. This phase corresponds to an onset of explosive instability. At a later stage the fourth order term can possibly cause saturation of the system, but this is beyond the goal of this model. The purpose of this model is to be able to identify the onset of explosive behavior, and thus identify explosively unstable plasma configurations.

There are systems with the special symmetries with the third order term identically zero. Under these circumstances our method does not work, and they must be investigated using alternative methods.
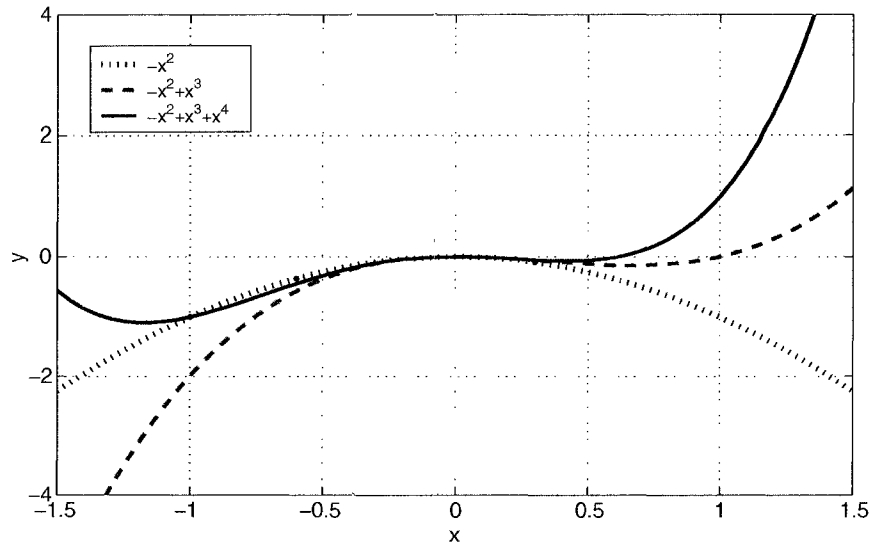
Figure 2.3: Comparison of terms of polynomial $-x^2 + x^3 + x^4$.

Figures 2.3 and 2.4 show comparison between a second, third and fourth order polynomials around $x_0 = 0$. Note the short interval of the third order term dominance in cases where all the terms have equal coefficients, but the long interval when a more restrictive condition is applied. Also, in this case the fourth order term causes the appearance of a double well, but in this situation this well is strongly asymmetric. This example demonstrates the fact

19
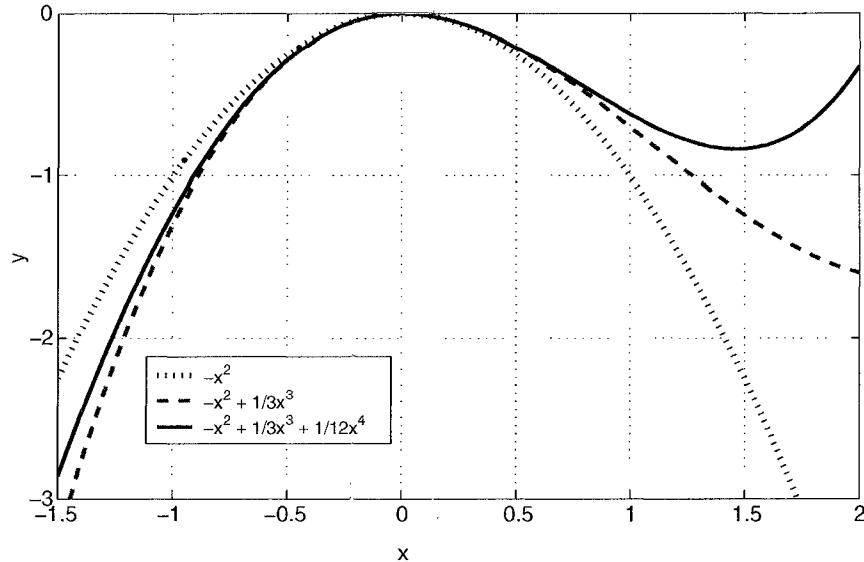
Figure 2.4: Comparison of terms of polynomial $-x^2 + 1/3x^3 + 1/12x^4$.

that we can safely identify explosive onset without consideration of the fourth order term.

There is one more thing we should consider in the ordering. Each of the higher orders in the expansion means analysis of the dynamics on shorter and shorter spatial scales. Therefore, to analyze higher order terms, these small scale effects (for instance Larmor radius effects) would have to be incorporated into the Lagrangian of the system we investigate. To conclude, since we are interested only in the identification of the onset of explosive instability, we do not need to consider the fourth order term in our analysis. After the third order term becomes dominant the perturbation ordering is violated and analysis of the full nonlinear dynamics is needed. This is beyond the objective of our model.

2.3 Ideal Magnetohydrodynamics

Here we demonstrate an application of this general method in ideal MHD. Then in the next chapter we will show practical demonstrations of the investigation of non-linear instabilities in both Cartesian and curvilinear coordinates. We used standard notation common in literature, the detailed list of the symbols used is in the Appendix.

2.3.1 Lagrangian in Ideal Magnetohydrodynamics

Although ideal MHD (see for instance [Nicholson, 1983]) is one of the simplest approximations of plasmas, it still describes some very interesting physical features of the plasma. Due to the relative simplicity of this description it is a useful tool for the development of

20

new formalisms that can be extended beyond ideal MHD. The Lagrangian of ideal MHD has the form

$$L = \int dV \left(\frac{1}{2}\rho v^2 - \frac{P}{\gamma - 1} - \frac{1}{2}B^2 \right). \tag{2.15}$$

This Lagrangian needs to be supplemented with constraints in order to yield non-trivial behavior. The commonly used constraints are mass conservation (2.16), magnetic flux conservation (2.17), and the adiabatic condition (2.18):

$$\int \rho dV = const, \tag{2.16}$$

$$\int B \cdot dS = const, \tag{2.17}$$

$$P\rho^{-\gamma} = const. \tag{2.18}$$

In the Lagrangian (2.15) we introduce the plasma displacement in the form of a coordinate shift (2.10), which is function of coordinates and time. Then the whole perturbation calculus can be performed in a geometrical framework, without introducing any new physical constraints on the system. Using the geometrical approach also brings the advantage that the results are independent of the coordinate system and hold for any geometry. Furthermore, this approach does not limit the physics beyond limitations introduced by ideal MHD.

2.3.2 Kinetic Energy

The perturbed velocity has the same form $\hat{v} = d\hat{x}/dt$ as the unperturbed velocity, with the difference that the plasma displacement is also an explicit function of x and therefore total differentiation is necessary. Taking into account the mass conservation law (2.16), and the fact that

$$d\hat{V} = JdV, \tag{2.19}$$

one obtains a density transformation rule of the form

$$\hat{\rho} = \rho/J, \tag{2.20}$$

where J is the Jacobian of the coordinate change (2.10). Then the perturbed kinetic energy has the form

$$\hat{K} = \int dV \frac{1}{2}\rho \left(v + \partial_t \xi + v^j \partial_j \xi \right)^2. \tag{2.21}$$

In the absence of ambient convection the first and the third terms in brackets vanish and the kinetic energy is simply

$$\hat{K} = \int dV \frac{1}{2}\rho(\partial_t \xi)^2. \tag{2.22}$$

This will be the form of the kinetic energy used throughout the rest of our work.

21

2.3.3 Thermal and Magnetic Energy

Since the mass conservation (2.16) combined with the rule for the transformation of a volume element (2.19) yields expression (2.20) for plasma density, applying the adiabatic condition (2.18), which connects density and pressure, the expression

$$\hat{P} = PJ^{-\gamma} \tag{2.23}$$

for the transformation of the pressure is obtained.

Similarly, since a surface element dS transforms as

$$\hat{dS_i} = A_i^j dS_j, \tag{2.24}$$

where

$$A_j^i = 3\delta_{jmn}^{ikl} J_k^m J_l^n, \tag{2.25}$$

and $J_b^a = \hat{x}_{,b}^a$ is the Jacobian matrix of the transformation (2.10), magnetic flux conservation (2.17) yields

$$\hat{B}^i = (A^{-1})_j^i B^j \tag{2.26}$$

for the transformation of the magnetic field. The derivation of expression (2.24) is shown in section 2.3.5. Consequently, the potential energy terms are

$$\hat{E}_T = \int dV \frac{PJ^{1-\gamma}}{\gamma - 1} \tag{2.27}$$

for the thermal component, and

$$\hat{E}_M = \int dV \frac{1}{2} J g_{ij} (A^{-1})_k^i B^k (A^{-1})_l^j B^l \tag{2.28}$$

for the magnetic part. The term g_{ij} is the metric tensor of the coordinate system and is necessary for the scalar product in the magnetic energy term.

2.3.4 Perturbed Lagrangian

Therefore, combining expressions (2.22), (2.27), and (2.28), the perturbed Lagrangian in the absence of convection is

$$\hat{L} = \int dV \left(\frac{1}{2} \rho (\partial_t \xi)^2 - \frac{PJ^{1-\gamma}}{\gamma - 1} - \frac{1}{2} J g_{ij} (A^{-1})_k^i B^k (A^{-1})_l^j B^l \right). \tag{2.29}$$

So far our results are consistent with those derived by Pfirsch and Sudan [1993]. However, our method of derivation of the Jacobian and the matrix A differs significantly. The method we will present in the next section is self consistent, purely geometrical, and does

not require any additional physical assumptions. The use of the component formalism and the use of generalized Kronecker deltas and Levi-Civita symbols ensures a very compact form of the results making further calculations much simpler. Also, Pfirsch and Sudan made the error of assuming that the inverse matrix A^{-1} is second order in the plasma displacement. Although this is true for the matrix A, it is not true for the matrix A^{-1}. Due to the omission of these terms, their expression for the third order perturbation in the Lagrangian (2.29) cannot be generally correct. In the situations with special symmetries (as were those that Pfirsch and Sudan discussed), the third order term is trivial, and also all these additional terms that they must have omitted are zero as well. However, due to the very complicated expression for the third order energy in their paper, direct comparison of their results with ours is extremely difficult. A major advantage of the formalism we use is that in situations with special symmetries many terms disappear due to their symmetry properties, reducing the complexity of calculations.

2.3.5 Transformation of Volume and Surface

Starting from the definition of the Jacobian $J = \det(\hat{x}^i_{,k})$, and using the definition of the determinant utilizing generalized Kronecker delta (see Section 2.4)

$$\det A^i_k = \delta(n)\underbrace{A \cdots A}_{n}, \tag{2.30}$$

the expression

$$\begin{aligned}
J &= \delta^{ijk}_{lmn}(\delta^l_i + \xi^l_{,i})(\delta^m_j + \xi^m_{,j})(\delta^n_k + \xi^n_{,k}) = \\
&= 1 + \xi^i_{,i} + \xi^i_{[,i}\xi^j_{,j]} + \xi^i_{[,i}\xi^j_{,j}\xi^k_{,k]}
\end{aligned} \tag{2.31}$$

for the Jacobian of the transformation (2.10) is obtained.

The surface element is defined as

$$dS_i = \epsilon_{ijk}dx^j dx^k. \tag{2.32}$$

Using this definition for the perturbed surface and noting that

$$d\hat{x}^j = (\delta^j_k + \xi^j_{,k})dx^k, \tag{2.33}$$

and using the fact that a product of a symmetric and an antisymmetric tensor is zero, the expression

$$\begin{aligned}
d\hat{S}_i &= 3\delta^{lmn}_{ijk}(\delta^j_m + \xi^j_{,m})(\delta^k_n + \xi^k_{,n})\epsilon_{lop}dx^o dx^p \equiv \\
&\equiv 3\delta^{lmn}_{ijk}(J^{-1})^j_m(J^{-1})^k_n \equiv A^l_i dS_l
\end{aligned} \tag{2.34}$$

23

for the transformation of a surface element is obtained. However, for the transformation of the magnetic energy the inverse matrix A^{-1} is needed. This inverse matrix has the same form as the matrix A

$$
\begin{aligned}
(A^{-1})^i_j &= 3\delta^{ikl}_{jmn}(\delta^m_k + \xi^m_{,k})^{-1}(\delta^n_l + \xi^n_{,l})^{-1} \equiv \\
&\equiv 3\delta^{ikl}_{jmn}(J^{-1})^m_k(J^{-1})^n_l.
\end{aligned}
\tag{2.35}
$$

The inverse Jacobian matrix is by definition expressed as

$$
(J^{-1})^i_j \equiv (3/J)\delta^{ikl}_{jmn}J^m_k J^n_l.
\tag{2.36}
$$

Expanded up to the third order it takes the form

$$
(J^{-1})^i_j = \delta^i_j - \xi^i_j + \xi^i_l\xi^l_j - \xi^i_l\xi^l_k\xi^k_j + O(\xi^4).
\tag{2.37}
$$

It is trivial to show that $J \cdot J^{-1} = 1$. Substituting this definition into (2.35) and expanding the results up to the desired order one can obtain the inverse matrix A^{-1} to arbitrary accuracy. The expansion up to the third order yields

$$
\begin{aligned}
(A^{-1})^i_j &= \delta^i_j + \xi^i_{,j} - \delta^i_j\xi^a_{,a} - \xi^i_{,j}\xi^a_{,a} + \frac{1}{2}\delta^i_j\left(\xi^a_{,a}\xi^b_{,b} + \xi^a_{,b}\xi^b_{,a}\right) - \\
&- \delta^i_j\xi^a_{,a}\xi^b_{,c}\xi^c_{,b} + \xi^i_{,j}\xi^a_{,b}\xi^b_{,a} + \xi^i_{,a}\xi^a_{,j}\xi^b_{,b} - \xi^i_{,a}\xi^a_{,b}\xi^b_{,j} + O(\xi^4).
\end{aligned}
\tag{2.38}
$$

Again, it is trivial to show that $A^{-1} \cdot A = 1$.

Equivalent results for the transformation of the magnetic field could be obtained in this special case by using the Lundquist identity, which can be written in the form $\hat{B}^i = B^j(\delta^i_j + \xi^i_{,j})/J$ [Lundquist, 1951]. Instead, we derived this relation directly from the magnetic flux conservation to demonstrate this method in its most general sense, with the direct use of the constraint to the Lagrangian (2.15).

2.3.6 Expansion of Potential Energy

Since the kinetic energy term in the Lagrangian (2.29) is second order, it is necessary to expand only the potential energy term. We substitute expressions for the Jacobian (2.31) and A^{-1} (2.38) into the expressions for the thermal (2.27) and the magnetic energies (2.28).

Substituting expression (2.31) into expression (2.27) and using a Taylor series expansion

$$
(1 + j)^{1-\gamma} = 1 + (1 - \gamma)j - (1/2)\gamma(1 - \gamma)j^2 + (1/6)\gamma(1 - \gamma^2)j^3
\tag{2.39}
$$

24

in (2.27), we obtain the expression for the thermal component of the potential energy up to third order in the form

$$\hat{E}_T = \int dV \frac{p}{\gamma - 1}\left[1 + (1 - \gamma)\left(\xi^i_{,i} + \xi^{[i}_{,i}\xi^{j]}_{,j} + \xi^{[i}_{,i}\xi^j_{,j}\xi^{k]}_{,k}\right) + \right.$$
$$\left. + \frac{\gamma(\gamma - 1)}{2}\left(\xi^i_{,i}\xi^j_{,j} + 2\xi^i_{,i}\xi^{[j}_{,j}\xi^{k]}_{,k}\right) + \frac{\gamma(1 - \gamma^2)}{6}\xi^i_{,i}\xi^j_{,j}\xi^k_{,k}\right]. \qquad (2.40)$$

The magnetic component of the potential energy doesn't contain any additional terms. After substituting expressions (2.31) and (2.38) into (2.28) we obtain for the magnetic energy

$$\hat{E}_M = \int dV \left[\frac{1}{2}\boldsymbol{B}^2\left(1 - \xi^i_{,i} + \frac{1}{2}(\xi^i_{,i}\xi^j_{,j} + \xi^i_{,j}\xi^j_{,i}) + \xi^i_{[,i}\xi^j_{,j}\xi^k_{,k]} + \xi^i_{,i}\xi^j_{,k}\xi^k_{,j}\right) + \right.$$
$$+ g_{ij}B^i B^l \left(\xi^j_{,l}(1 - \xi^k_{,k} + \xi^k_{,m}\xi^m_{,k}) + \xi^j_{,k}\xi^k_{,l}\xi^m_{,m} - \xi^j_{,k}\xi^k_{,m}\xi^m_{,l}\right) + $$
$$\left. + \frac{1}{2}g_{ij}B^k B^l \xi^i_{,k}\xi^j_{,l}(1 - \xi^m_{,m})\right]. \qquad (2.41)$$

The magnetic energy contains two components, the first one is due to magnetic pressure, the second one is due to curvature. Unlike the use of a traditional vector formalism, use of the component notation prevents us from having terms that cancel or add. These terms can add much complexity to a vector formalism as in this formalism it is often not clear just which terms cancel or add. Therefore the number of terms is significantly reduced in the geometrical formalism, and also the expressions are in "ready to use" form. Also, this notation immediately distinguishes between the terms due to the magnetic pressure and the terms due to the curvature.

2.3.7 Expansion of Lagrangian, Interpretation of Terms

Using the expressions (2.22), (2.40), and (2.41) it is possible to expand the Lagrangian (2.29) with respect to the plasma displacement as

$$\hat{L} = \int dV \left(\mathcal{L}^0 + \mathcal{L}^1(\xi) + \mathcal{L}^2(\xi^2) + \mathcal{L}^3(\xi^3) + \cdots\right), \qquad (2.42)$$

where $\mathcal{L}$ denotes Lagrangian density.

25

The terms $\mathcal{L}^0$ - $\mathcal{L}^3$ are:

$$\mathcal{L}^{(0)} = -\frac{P}{\gamma - 1} - \frac{1}{2}\boldsymbol{B}^2, \tag{2.43}$$

$$\mathcal{L}^{(1)} = \left(P + \frac{1}{2}\boldsymbol{B}^2\right)\xi^k_{,k} - g_{ij}B^iB^l\xi^j_{,l}, \tag{2.44}$$

$$\mathcal{L}^{(2)} = \frac{1}{2}\Big[\rho(\partial_t\xi)^2 - P\Big((\gamma - 1)\xi^a_{,a}\xi^b_{,b} + \xi^a_{,b}\xi^b_{,a}\Big) -$$
$$- g_{ij}B^kB^l\xi^i_{,k}\xi^j_{,l} + 2g_{ij}B^iB^l\xi^j_{,l}\xi^k_{,k} -$$
$$- \frac{1}{2}\boldsymbol{B}^2\Big(\xi^a_{,a}\xi^b_{,b} + \xi^a_{,b}\xi^b_{,a}\Big)\Big], \tag{2.45}$$

$$\mathcal{L}^{(3)} = P\Big(\xi^{[a}_{,a}\xi^b_{,b}\xi^{c]}_{,c} - \gamma\xi^a_{,a}\xi^{[b}_{,b}\xi^{c]}_{,c} + \frac{\gamma(1 + \gamma)}{6}\xi^a_{,a}\xi^b_{,b}\xi^c_{,c}\Big) -$$
$$- \frac{1}{2}\boldsymbol{B}^2\Big(\xi^{[a}_{,a}\xi^b_{,b}\xi^{c]}_{,c} + \xi^a_{,a}\xi^b_{,c}\xi^c_{,b}\Big) + \frac{1}{2}g_{ij}B^kB^l\xi^i_{,k}\xi^j_{,l}\xi^a_{,a} -$$
$$- g_{ij}B^iB^l\Big(\xi^j_{,l}\xi^a_{,b}\xi^b_{,a} + \xi^j_{,a}\xi^a_{,l}\xi^b_{,b} - \xi^j_{,a}\xi^a_{,b}\xi^b_{,l}\Big). \tag{2.46}$$

Using the variational principle in the first and the second order terms of the Lagrangian (2.42) it is possible to derive equations governing dynamics of the plasma in a linear approximation (the equilibrium condition and the equation of motion). The condition

$$\int dV\mathcal{L}^{(1)} = 0 \tag{2.47}$$

yields the equilibrium condition for ideal MHD in the form

$$-\left(p + \frac{1}{2}\boldsymbol{B}^2\right)_{,i} + g_{il}B^jB^l_{,j} = 0. \tag{2.48}$$

This is a standard equation relating the sum of gradients of thermal and magnetic pressure and pressure due to field-line curvature. Often, it is highly non-trivial to find equilibrium solution satisfying condition (2.48).

The condition

$$\int dV\mathcal{L}^{(2)} = 0 \tag{2.49}$$

yields the equation of motion for plasma in a linear approximation in the form

$$\rho\partial_{tt}\xi_i = \partial_i\Big(\gamma P\frac{1}{\sqrt{g}}\partial_l\sqrt{g}\xi^l + \xi^l\partial_lP - g_{lk}B^k\frac{1}{\sqrt{g}}\partial_p\sqrt{g}(\xi^lB^p - \xi^pB^l)\Big) +$$
$$+ B^l\partial_l\Big(\frac{g_{ij}}{\sqrt{g}}\partial_p\sqrt{g}(\xi^jB^p - \xi^pB^j)\Big) - (\partial_iB^l)\frac{g_{lj}}{\sqrt{g}}\partial_p\sqrt{g}(\xi^jB^p - \xi^pB^j) +$$
$$+ (\partial_iB_l - \partial_lB_i)\Big(\frac{1}{\sqrt{g}}\partial_p\sqrt{g}(\xi^lB^p - \xi^pB^l)\Big). \tag{2.50}$$

Equation (2.50) is a wave equation describing a linear wave propagating in a plasma, for which ideal MHD is a reasonable approximation. There are no further restrictions on the

26

direction of propagation nor on the configuration of the ambient quantities for this equation to hold. The only restrictions on the validity of the equation (2.50) are that the amplitude of the perturbation, and the gradients of the perturbation be small enough for a linear approximation to be reasonable. However, by applying certain restrictions to this equation, it is possible to derive dispersion relations for specific plasma configurations, as we will show next. The same equation can also be derived directly from the ideal MHD equations using a formalism of differential forms as we show at the end of this chapter.

2.3.8 Examples of Linear Plasma Behavior in Ideal Magnetohydrodynamics

In this section we present a derivation of several dispersion relations for specific plasma configurations to demonstrate the simplicity of the use of equation (2.50), and also consistency of this formalism with previous work in this area.

Waves in Homogeneous Plasma

In the case of a homogeneous magnetic field, and assuming harmonic time and space dependence, equation (2.50) becomes

$$\omega^2 \xi^i = C_S^2 k^i k_l \xi^l - \frac{B_j}{\rho_0 \mu_0} k^i k_p (\xi^j B^p - \xi^p B^j) + \frac{B^l}{\rho_0 \mu_0} k_l k_p (\xi^i B^p - \xi^p B^i). \tag{2.51}$$

Since we have freedom in the choice of coordinates, we choose them such that

$$\begin{aligned} \boldsymbol{B} &= (B_x, B_y, 0), \\ \boldsymbol{k} &= (k, 0, 0). \end{aligned}$$

Equation (2.51) splits into one equation for the displacement perpendicular to the ambient magnetic field and two equations for the displacement in the plane of the magnetic field. The latter two equations can then be combined into one equation. So the final two equations are:

$$0 = \xi_z \left(1 - \frac{k^2 V_{Ax}^2}{\omega^2} \right), \tag{2.52}$$

$$0 = \xi_x \left\{ 1 - \frac{k^2 V_{Ax}^2}{\omega^2} - \frac{k^2}{\omega^2} \left[(V_S^2 + V_{Ay}^2) \left(1 - \frac{k^2 V_{Ax}^2}{\omega^2} \right) + \frac{V_{Ax}^2 V_{Ay}^2}{\omega^2} k^2 \right] \right\}, \tag{2.53}$$

27

where

$$V_S^2 = \frac{\gamma P}{\rho}, \tag{2.54}$$

$$V_{Ax}^2 = \frac{B_x^2}{\rho}, \tag{2.55}$$

$$V_{Ay}^2 = \frac{B_y^2}{\rho}. \tag{2.56}$$

The first equation (2.52) yields the dispersion relation for the shear Alfvén wave, the second one (2.53) describes the fast and slow compressional modes. This result agrees with *Landau and Lifshitz* [1992].

Field Line Resonances

In the case of a rectilinear magnetic field the natural choice for the coordinates is a Cartesian coordinate system. Then the metric tensor

$$g_{ij} = \text{diag}(1, 1, 1), \tag{2.57}$$

and the vectors and covectors are identical. The equilibrium condition (2.48) takes the simple form

$$(P + \boldsymbol{B}^2/2)_{,i} = 0. \tag{2.58}$$

Applying condition (2.58) to equation (2.50), and assuming a harmonic time dependence, a momentum equation in the form

$$\begin{aligned}
\rho \omega^2 \xi^i &= -\partial^i \left((\gamma P + \boldsymbol{B}^2) \partial_l \xi^l - B_j B^p \partial_p \xi^j \right) - \\
&- B^l \partial_l \partial_p (\xi^i B^p - \xi^p B^i) - (\partial_j B^i) \partial_p (\xi^j B^p - \xi^p B^j)
\end{aligned} \tag{2.59}$$

is obtained. We now assume an orientation of the axes such that the z-axis is along magnetic field lines, and the variation of ambient quantities is along the x-axis. Then

$$\boldsymbol{B} = (0, 0, B(x)), \tag{2.60}$$

and all the derivatives of P, B, and ρ except ∂_x vanish. Assuming also that the displacement is harmonic along the y and z directions

$$\boldsymbol{\xi}(\boldsymbol{x}) = \boldsymbol{\xi}(x) \exp i(k_y y + k_z z), \tag{2.61}$$

equation (2.59) can be further reduced to

$$\rho(\omega^2 - k_z^2 V_A^2) \xi_x = -\partial_x (F(x) \partial_x \xi_x), \tag{2.62}$$

28

where the function $F(x)$ is defined as

$$F(x) = \frac{\rho(\omega^2 - k_z^2 V_A^2)(\omega^2 V^2 - V_A^2 V_S^2 k_z^2)}{\omega^2(\omega^2 - V^2 k^2) + k_z^2 k^2 V_A^2 V_S^2},$$ (2.63)

(2.64)

where

$$V_A^2 = \boldsymbol{B}^2/\rho,$$ (2.65)

$$V_S^2 = \gamma P/\rho,$$ (2.66)

$$V^2 = V_A^2 + V_S^2,$$ (2.67)

$$k^2 = k_y^2 + k_z^2.$$

This result is consistent with the expression obtained by *Harold and Samson* [1992]. Equation (2.62) yields two turning points and two resonances [*Stix*, 1992]. In the case of a cold plasma expression (2.63) reduces to

$$F(x) = \frac{\rho V_A^2(\omega^2 - k_z^2 V_A^2)}{\omega^2 - (k_z^2 + k_y^2)V_A^2}.$$ (2.68)

This equation has only one turning point and one resonance at the point where

$$\omega^2 = k_z^2 V_A^2.$$ (2.69)

The occurrence of this resonance is due to the coupling between a compressional Alfvén wave and a shear Alfvén wave of the same frequency. Since there is no curvature, and we considered only the situation with no gravity, a ballooning mode cannot evolve in this configuration, and thus this mode cannot be explosively unstable. We will give more details on ballooning models in the next section. In the next chapter we will show results from numerical models of the FLRs including also the energy transfer in this mode as a simple example of a stability investigation.

Linear Ballooning Mode

A more interesting model assumes a general curved magnetic field, with the orthonormal coordinate system defined

$$\hat{e} = \boldsymbol{B}/B,$$ (2.70)

$$\hat{n} = R_c \hat{e} \cdot \nabla \hat{e},$$ (2.71)

$$\hat{\phi} = \hat{e} \times \hat{n}.$$ (2.72)

29

Here again the metric is $g_{ij} = \text{diag}(1, 1, 1)$, and vectors and covectors are identical. Introducing the definitions

$$\kappa_p = \hat{n} \cdot \nabla \ln P, \tag{2.73}$$

$$\kappa_b = \hat{n} \cdot \nabla \ln B, \tag{2.74}$$

$$\kappa_c = \hat{n} \cdot (\hat{e} \cdot \nabla)\hat{e} \tag{2.75}$$

the equilibrium condition (2.48) can be written in components as

$$\partial_{\|} P = 0, \tag{2.76}$$

$$\frac{V_S^2}{\gamma V_A^2} \kappa_p = \kappa_c - \kappa_b, \tag{2.77}$$

$$\partial_\phi P = 0. \tag{2.78}$$

Assuming no azimuthal dependence ($\partial_\phi = 0$) of the ambient field, the problem reduces to two dimensions. Equation (2.50) can be split into components in the parallel and radial directions. Assuming that the ambient magnetic field changes slowly along the field lines, and consequently assuming a harmonic dependence of the displacement along the field lines (i.e. $\partial_{\|} \to ik_{\|}$), and in time (i.e. $\partial_t \to -i\omega$), the parallel component of equation (2.50) is simplified to

$$\xi_{\|} = -ik_{\|} \frac{V_S^2}{\omega^2} \partial_l \xi^l. \tag{2.79}$$

Subsequently, assuming very small scale sizes in the azimuthal direction ($k_\phi \to \infty$), which is equivalent to averaging the total perturbation pressure $P_T = \delta p + \boldsymbol{B} \cdot \delta \boldsymbol{B}$ to zero [Liu, 1997], which in the terms of equation 2.50 is

$$P_T \equiv \gamma P \partial_l \xi^l + \xi^l \partial_l P - B_l \partial_p (\xi^l B^p - \xi^p B^l) = 0, \tag{2.80}$$

and using equation (2.79) the equation

$$\left(V_S^2 + V_A^2 - \frac{V_A^2 V_S^2 k_{\|}^2}{\omega^2} \right) \partial_j \xi^j = -2\kappa_c V_A^2 \xi_n, \tag{2.81}$$

connecting compressional and shear Alfvén wave, is obtained.

The radial component of equation (2.50) in the absence of the perturbation pressure is simply

$$\left[\omega^2 - V_A^2 k_{\|}^2 - 2V_A^2 \kappa_c (\kappa_b + \kappa_c) \right] \xi_n =$$

$$2\kappa_c V_A^2 \left(1 - \frac{V_S^2 k_{\|}^2}{\omega^2} \right) \partial_j \xi^j. \tag{2.82}$$

30

This equation describes the generation of the shear Alfvén wave by the compressional wave.

Equations (2.81) and (2.82) describe a linear ballooning mode, and are consistent with results obtained by Liu [1997].

The examples above illustrate that our geometrical method leads easily to several classic results in MHD. Later we consider more interesting non-linear problems.

2.4 Ideal Magnetohydrodynamics and Differential Forms

2.4.1 Differential Forms

There is also an alternative way of introducing differential geometry into fluid dynamics and MHD. The behavior of the fluid can be easily described in terms of differential forms, see *Flanders* [1963], pg 188. In the following paragraphs we provide a brief description of differential forms and operators acting on the space of forms. For more detailed treatment see e.g [*Schutz*, 1980].

Definition of Differential Forms

A differential form is defined as the multilinear mapping from the vector space $L \times \cdots \times L \to$ $\boldsymbol{R}$, antisymmetric in all its components, where L is an arbitrary vector space and $\boldsymbol{R}$ is the space of real numbers. The differential form is usually called a p-form, where p is the rank of the form. It is obvious that in an n-dimensional space all the p-forms with $p > n$ must be zero. It is also clear that in an n-dimensional space only one linearly independent n-form can exist. This form is often called the form of volume and has the general definition

$$\omega = f(\boldsymbol{x})\epsilon_{i...j}dx^i \wedge \ldots \wedge dx^j. \tag{2.83}$$

The exact meaning definition of the operator $\wedge$ is explained later in the subsection on operators on differential form. In case of a metric space (which is usually the case with physical problems) the form of volume (2.83) becomes

$$\omega = \sqrt{g}\epsilon_{i...j}dx^i \wedge \ldots \wedge dx^j, \tag{2.84}$$

where $g = \det(g_{ij})$ is the determinant of the metric tensor and $\epsilon_{i...j}$ is the fully antisymmetric unit tensor.

31

Generalized Kronecker Deltas

In analogy with the Kronecker delta δ^i_j one can introduce a tensor $\delta^{a\cdots b}_{c\cdots d}$ working on differential forms the same way as δ^i_j works on tensors:

$$\delta^{a\cdots b}_{c\cdots d}\alpha_{a\cdots b} = \alpha_{c\cdots d}, \tag{2.85}$$

where α is an arbitrary differential form. Since differential forms are antisymmetric, it is clear that $\delta^{a\cdots b}_{c\cdots d}$ must be an antisymmetric combination of the ordinary deltas:

$$\delta^{a\cdots b}_{c\cdots d} = \delta^a_{[c}\cdots\delta^b_{d]}. \tag{2.86}$$

It is sufficient to perform the antisymmetrization in the lower (upper) indices. Due to the form of Kronecker delta it will also be antisymmetric in the upper (lower) indices. We can also prove that the generalized delta is connected to the fully antisymmetric tensor $\epsilon_{a\cdots b}$ as

$$\delta^{i\cdots j}_{k\cdots l} = \frac{1}{n!}\epsilon^{i\cdots j}\epsilon_{k\cdots l}. \tag{2.87}$$

Often, instead of writing all the indices, a short form of the generalized delta, $\delta(p)$, where p denotes number of either lower or upper indices, is used.

Also, contractions of generalized deltas, $\delta^{a\cdots bc\cdots d}_{a\cdots bc\cdots f}$, can be treated very easily. These contractions are especially useful in the case of multi — crossproducts. The contraction of $\delta(p)$ in k indices in n-dimensional space is

$$\delta_k(p) = \frac{(p-k)!}{p!}\frac{(n-(p-k))!}{(n-p)!}\delta(p-k). \tag{2.88}$$

The generalized deltas are also very useful in dealing with determinants and inverse matrices. The expression for a determinant of an $n \times n$ matrix A is

$$\det A = \delta(n)\underbrace{A..A}_{n}, \tag{2.89}$$

and the expression for an inverse matrix is

$$A^{-1} = \frac{n!}{(n-1)!\det A}\delta(n)\underbrace{A..A}_{n-1}. \tag{2.90}$$

We have used both these expressions in the derivation of the transformation properties of the surface and the volume in the derivation of the perturbed Lagrangian (2.42).

32

Operators for Differential Forms

Here we present several useful operators in the space of differential forms.

- The wedge product (sometimes called the outer product) which is a generalization of the cross-product in the vector analysis

$$\alpha \wedge \beta = \frac{(p+q)!}{p!q!} \mathrm{Alt}(\alpha \otimes \beta),\tag{2.91}$$

α and β are p and q forms respectively, and Alt denotes antisymmetrization in all components.

- The inner product i_v is defined as

$$(i_V\alpha)\underbrace{(U,\cdots,W)}_{p-1} = \alpha\underbrace{(V,U,\cdots,W)}_{p}.\tag{2.92}$$

In the other words it is a contraction of p-form α with vector V. So if α is p-form, $i_V\alpha$ is $(p-1)$-form.

- The outer derivative $\tilde{d}$ is defined as

$$(\tilde{d}\boldsymbol{T})_{ij\cdots k} = (-1)^p(p+1)T_{[j\cdots k,i]},\tag{2.93}$$

which is an analogy of the gradient and curl. Obviously

$$\tilde{d}\tilde{d}\alpha = 0\tag{2.94}$$

for any α since the second derivative is symmetric.

- Another differential operator, working not only on differential forms, but on tensors in general, that proves to be very useful in fluid dynamics, is the Lie derivative. This is defined as the rate at which some quantity changes along the integral curves of some vector (for instance stream lines). The notation for the Lie derivative we use is $\mathcal{L}_{\bar{V}}$:

$$\mathcal{L}_{\bar{V}}T = \frac{d}{dt}(^*T)(\gamma(t)),\tag{2.95}$$

where $\gamma(t)$ is an integral curve of the vector V and * denotes here pull-back of the tensor T (Lie image of the tensor T at the origin of the curve γ).

- The operator star ($*$) can be defined as the application of the form of volume ω (2.83) on an arbitrary tensor

$$*T = \omega(T).\tag{2.96}$$

This operator allows the definition of divergence for differential forms.

33

These operators are defined without metric structure on the manifold we are dealing with. This makes these operators very universal and makes it possible to deal with the MHD equations without any knowledge of the geometry of the magnetic field. However, most of the real physical systems can be described by a metric geometry.

2.4.2 Magnetohydrodynamics in Terms of Differential Forms

Basic Equations

Now it is relatively straightforward to write equations for ideal MHD in terms of differential forms. To simplify the final expressions, we assume a metric space with the metric tensor g_{ij}. Then it is possible to introduce a notation $\tilde{T}$ for vectors and tensors with upper indices and $\tilde{B}$ for differential forms. The connection between them is

$$T^{i\cdots j} = g^{ik} \cdots g^{jl} T_{kl},$$ (2.97)

$$T_{i\cdots j} = g_{ik} \cdots g_{jl} T^{kl}.$$ (2.98)

Flanders [1963] presents expressions for the fluid dynamics (equations (2.99) and (2.102), and the non-magnetic part of equation (2.101)). It is straightforward to extend these expressions for the case of magnetized fluid. Also the equation describing the generation of magnetic fields by the flow of the fluid must be added. The MHD equations can then be written as:

$$(\partial_t + \mathcal{L}_{\tilde{v}}) * \rho = 0,$$ (2.99)

$$\partial_t \tilde{B} = *\tilde{d}(*\tilde{v} \wedge \tilde{B}),$$ (2.100)

$$\rho(\partial_t + \mathcal{L}_{\tilde{v}})\tilde{v} = -\tilde{d}P + \frac{\rho}{2}\tilde{d}v^2 - \frac{1}{\mu_0} * \tilde{B} \wedge (*\tilde{d}\tilde{B}),$$ (2.101)

$$P = P(\rho, s).$$ (2.102)

Equation (2.99) is the conservation of the mass

$$*\rho \equiv \rho dV.$$ (2.103)

This equation can be easily connected to the integral form of the continuity equation using the identity

$$\mathcal{L}_{\tilde{V}} \equiv \tilde{d}i_V + i_V \tilde{d}$$ (2.104)

and the generalized Stokes theorem

$$\int_{\partial \Sigma} \tilde{\alpha} = \int_{\Sigma} \tilde{d}\tilde{\alpha},$$ (2.105)

34

where α is an arbitrary form, $\tilde{d}$ is an outer derivative, Σ is some closed submanifold, and $\partial\Sigma$ is a boundary of the submanifold Σ.

Equation (2.100) is the induction equation where we just substituted a wedge product instead of a vector product. The third equation (2.101) is the momentum equation in which we substituted $\mathcal{L}_{\bar{v}}\tilde{v}$ for $\boldsymbol{v}.\nabla\boldsymbol{v}$. However, the Lie derivative contains additional term $\boldsymbol{v}.(\nabla\boldsymbol{v})$ which we had to subtract from the equation. The last equation is the equation of state. In the physics of the near-Earth magnetosphere it is often reasonable to assume adiabatic processes and then the equation of state is simply

$$\frac{d}{dt}\left(P\rho^{-\gamma}\right) = 0. \tag{2.106}$$

Linear Wave Equation

Linearizing equations (2.99) - (2.101) and (2.106) a linear wave equation in the form

$$\rho_0\partial_{tt}\tilde{\xi} \quad = \tilde{d}\left[\left(\gamma P_0 + \frac{B_0^2}{2\mu_0}\right)*\tilde{d}*\tilde{\xi} + \mathcal{L}_{\bar{\xi}}P_0 + \frac{\tilde{B}_0}{\mu_0}(\mathcal{L}_{\bar{\xi}}\bar{B}_0)\right] +$$

$$+\mathcal{L}_{\bar{B}_0}\tilde{X} - *\tilde{X}\wedge\left(*\tilde{d}\tilde{B}_0\right), \tag{2.107}$$

where

$$\tilde{X} \quad = \quad \frac{1}{\mu_0}*\tilde{d}*(\bar{\xi}\wedge\tilde{B}_0)$$

$$\bar{X} \quad = \quad -\frac{1}{\mu_0}\left(\mathcal{L}_{\bar{\xi}}\bar{B}_0 + \bar{B}_0(*\tilde{d}*\bar{\xi})\right)$$

is obtained. The first term on the right-hand-side now represents a gradient of the total perturbation pressure which is due to the flux of plasma (the first part) and a change of the background P_0 and B_0 along the displacement (the second part). The second term on the right-hand-side is a change of the magnetic field (perturbation plus a change of the unperturbed field) along the field line, this term contains the force due to field-line curvature. The last term is the Amperean force. $\bar{X}$ represents the change of the background field B_0 due to the plasma displacement $\bar{\xi}$.

Equation (2.107) can be rewritten in coordinates as

$$\rho_0\partial_{tt}\xi^i \quad = g^{ij}\partial_j\left(\gamma P_0\frac{1}{\sqrt{g}}\partial_l\sqrt{g}\xi^l + \xi^l\partial_l P_0\right) -$$

$$-g^{ir}g_{jl}\frac{B^l}{\mu_0}\partial_r\frac{1}{\sqrt{g}}\partial_p\sqrt{g}(\xi^j B^p - \xi^p B^j) + \frac{B^l}{\mu_0}\partial_l\frac{1}{\sqrt{g}}\partial_p\sqrt{g}(\xi^i B^p - \xi^p B^i) -$$

$$-\left(g^{il}\partial_l\frac{B^j}{\mu_0} - g^{jl}\partial_l\frac{B^i}{\mu_0}\right)\sqrt{g}g^{pq}\partial_q\frac{1}{\sqrt{g}}\xi^r B^s(g_{jr}g_{ps} - g_{pr}g_{js}). \tag{2.108}$$

This equation agrees with equation (2.50) obtained from the Lagrangian of ideal MHD using variational calculus.

35

Chapter 3

Numerical Modeling of the Instability Criteria

In this chapter we show an application of the ideal MHD model, developed in Chapter 2, to two plasma configurations in order to demonstrate the effectiveness of our method and its applicability not only at a theoretical level, but at a practical level as well.

3.1 Discussion of Numerical Approach

Both examples follow the same format:

- Initial equilibrium configuration is defined, so that equation (2.48) holds.

- Linear wave equation (2.50) is solved for the plasma displacement ξ.

- The second and the third order potential energy density is calculated using numerical solutions for plasma displacement and these energies are compared.

- Possible unstable areas are identified.

In both examples we used a cold plasma approximation ($P = 0$). We have done this to simplify the determination of an initial equilibrium. This is very helpful especially in curvilinear coordinates, where finding an initial equilibrium often presents quite a challenge.

The components of equation (2.50) to be solved can be written in a general form

$$\partial_t \xi_i = u_i, \tag{3.1}$$

$$\partial_t u_i = F(B, \rho; \xi, \partial \xi, \partial^2 \xi), \tag{3.2}$$

$$i = 1, 2, 3.$$

36

ξ and u are functions of two spatial variables and of time. The choice of coordinate system and form of equations (3.1) and (3.2) for different coordinates are discussed separately for a box and curvilinear systems.

We use 2-dimensional models. We assume a harmonic dependence of the plasma displacement in one direction and solve differential equations in the remaining two directions. This does not limit the physics too significantly, since most real physical systems, including those in magnetospheric plasmas, will have some kind of symmetry. This assumption also allows us to obtain results from computational models using reasonable resources.

The most effective numerical method for our problem proved to be a simple predictor – corrector method of the second order (for detailed description see [*Rickard and Wright*, 1994]). We also tried fourth order Runge–Kutta methods and staggered leapfrog methods, but these two methods were extremely inefficient for our problems, requiring approximately 1,000 to 10,000 times smaller time-step, compared to predictor–corrector, to keep the solution stable. This puts unreasonable stresses on the computational resources that are needed. For the detailed discussion of these methods see e.g. [*Press et. al.*, 1992].

We use an implicit time scheme, and centered differentiation

$$\frac{df}{dx} = \frac{f_{n+1} - f_{n-1}}{2\Delta x} \tag{3.3}$$

for spatial derivatives.

3.2 Plasma in a Box: Field Line Resonances

In this section we present an example of a negative case of non-linear plasma instability investigation. In the absence of magnetic field curvature, and in the absence of gravity, it is impossible for ballooning modes to evolve (see e.g. [*Hameiri et. al.*, 1991] and [*Ohtani and Tamao*, 1993]). Therefore this example provides a test for our method in a configuration where the results are known apriori. As was already mentioned, we confined ourselves to an investigation of cold plasma due to the simplicity of the initial equilibrium.

3.2.1 Basic Equations

In the absence of field-line curvature the linear wave equation (2.50) simplifies significantly. Assuming axes orientation such that the ambient magnetic field B is directed along the z-axis, the equation describing wave propagation in a cold plasma in a box can be written

37

in components

$$\partial_t \xi_i = u_i, \qquad i = x, y, z, \tag{3.4}$$

$$\partial_t u_x = V_A^2 \partial_x (\partial_x \xi_x + \partial_y \xi_y) + V_A^2 \partial_{zz}^2 \xi_x, \tag{3.5}$$

$$\partial_t u_y = V_A^2 \partial_y (\partial_x \xi_x + \partial_y \xi_y) + V_A^2 \partial_{zz}^2 \xi_y, \tag{3.6}$$

$$\partial_t u_z = 0, \tag{3.7}$$

where the Alfvén velocity is defined as $V_A^2 = B^2/\rho$. The perpendicular dynamics is decoupled from the parallel. Since the motion along a field line is constant, we can safely assume $\xi_z \equiv 0$. The configuration of the plasma box is shown in Fig. 3.1.
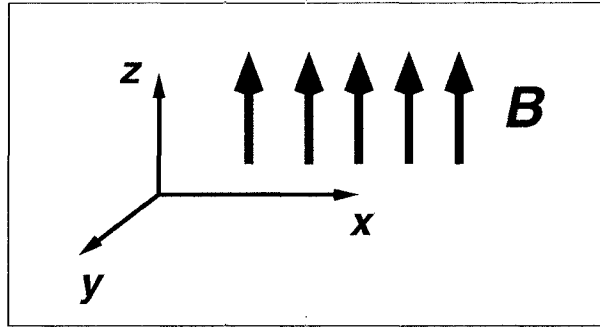

Figure 3.1: Configuration for the plasma in a box. The z-axis is directed along magnetic field.

FLR's occur when the compressional wave and the shear Alfvén wave are coupled. From equations (3.5) to (3.7) it follows that this coupling is only possible when the azimuthal wave number is non-zero. The system of equations (3.4) to (3.7) was solved in the xy-plane. The initial configuration was chosen to match the one used by *Rickard and Wright* [1994], so that we would be able to test our results by a comparison with their results.

Initial Configuration

We used a box $0 < x < 1$ and $0 < y < 15$ with a grid 64 (x direction) $\times$ 128 (y direction). The time-step was chosen to be $dt = 0.001$ and the runtime $0 < t < 25$. The wave-number along field lines was $k_z = \pi$. The ambient quantities were magnetic field $B = 1$ and plasma density defined as ρ_0/V_A^2 with $\rho_0 = 1$, and $V_A = 1 - x/\varphi$; $\varphi = 1.3$. (See Figures 3.2 and 3.3.) In the simulation we used open boundary conditions, where derivatives of the plasma displacement and velocity were put to zero. In fact, the boundary condition at the far end of the box in the y-direction is not important, since the range of y values was chosen to be large enough so that the perturbation would not reach the end of the box.
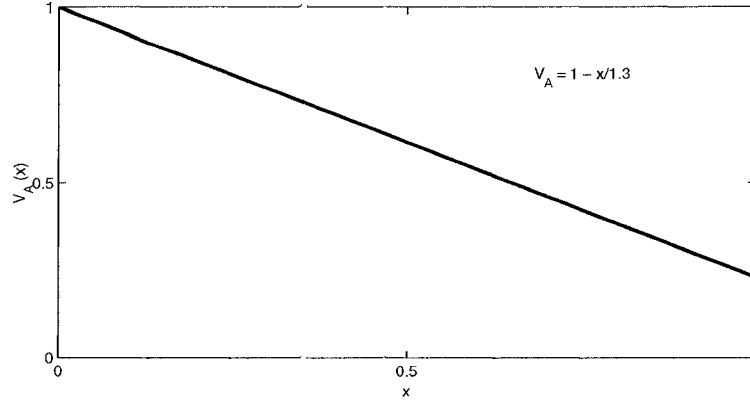
38

Figure 3.2: Alfvén velocity profile for the box for the FLRs example.

The initial displacement and velocity were chosen to be

$$\xi_{i0} \;=\; 0, \qquad i = x, y, z, \tag{3.8}$$

$$u_{i0} \;=\; 0, \qquad i = y, z, \tag{3.9}$$

$$u_{x0} \;=\; \Lambda \sin\left(\frac{2\pi x}{L_x}\right)\left[1 + \cos\left(\frac{\pi y}{L_y}\right)\right], \qquad y \leq 1, \tag{3.10}$$

$$u_{x0} \;=\; 0, \qquad y > 1, \tag{3.11}$$

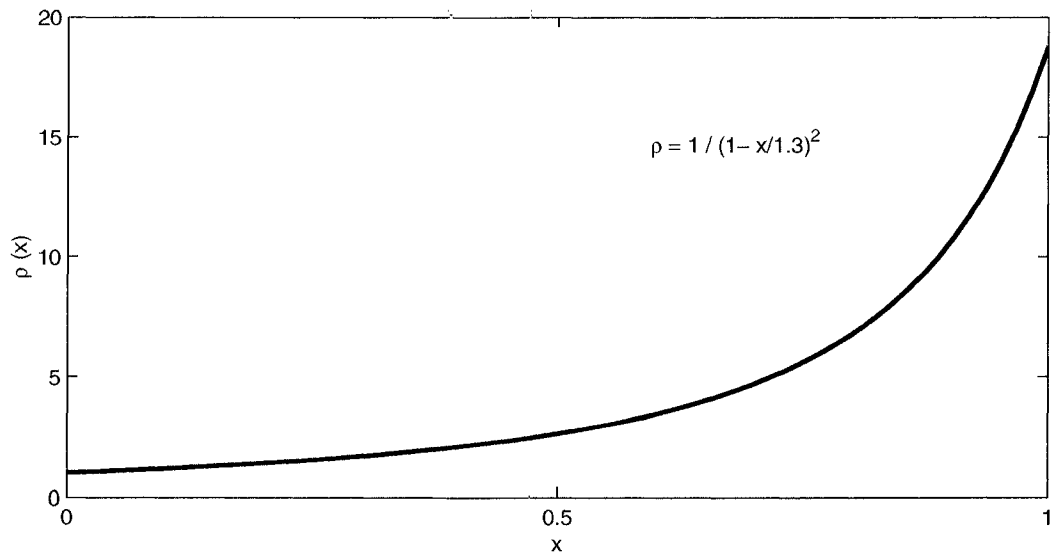where $\Lambda = 0.5, L_x = 2$, and $L_y = 1$. (See Figure 3.4.)

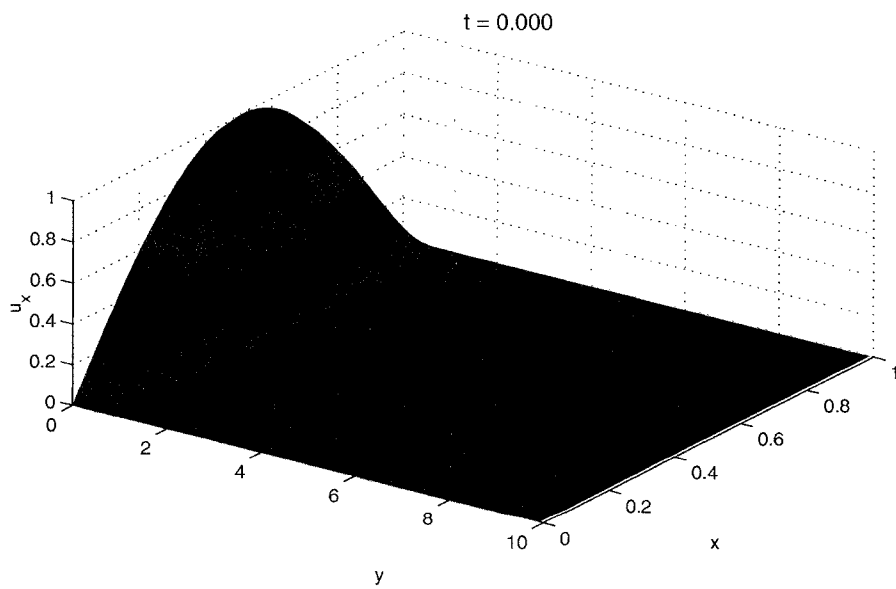Figure 3.3: Corresponding plasma density profile for a linear Alfvén velocity dependence.

Figure 3.4: Initial radial velocity (u_x) profile.

40

Results

Our results match those obtained by *Rickard and Wright* [1994]. The comparison was done for the shape and magnitude for corresponding cross sections of the velocity. We also compared the frequency of the eigenmodes using Fourier analysis of the velocity, and the position of the resonance. All these results matched the results obtained by Rickard and Wright. The evolution of the modes is illustrated in Figures 3.5 and 3.6.

Using the numerical solutions of equations (3.4) to (3.7) in the expressions for energy density from the Lagrangian (2.42), maps of the second and the third order potential energy density were obtained. Examples of maps for $t = 25$ are shown in Fig. 3.7. Figures 3.8 and 3.9 present profiles of the energy density at $y = 0.83$ (maximum value of energy density) at times $t = 5$ and $t = 25$. The energy density evolves to a localized region at the point of resonance, and the second order energy dominates at all times for the temporal interval we investigated. Since the values of the energy density in each order are of the same order of magnitude, and the slight increase is to be ascribed to the localization of the peak, we can assume that the relation $W^{(3)} \ll W^{(2)}$ holds at all times. Thus the system is stable as predicted.

Though this example is extremely simple, it serves to illustrate the fact that our derivation of the Lagrangian (2.15) up to the third order when used in numerical models gives robust results. Although it has not provided any new physical insights, this test is very important for the evaluation of the method when used with more complicated models where the result is not apriori known.
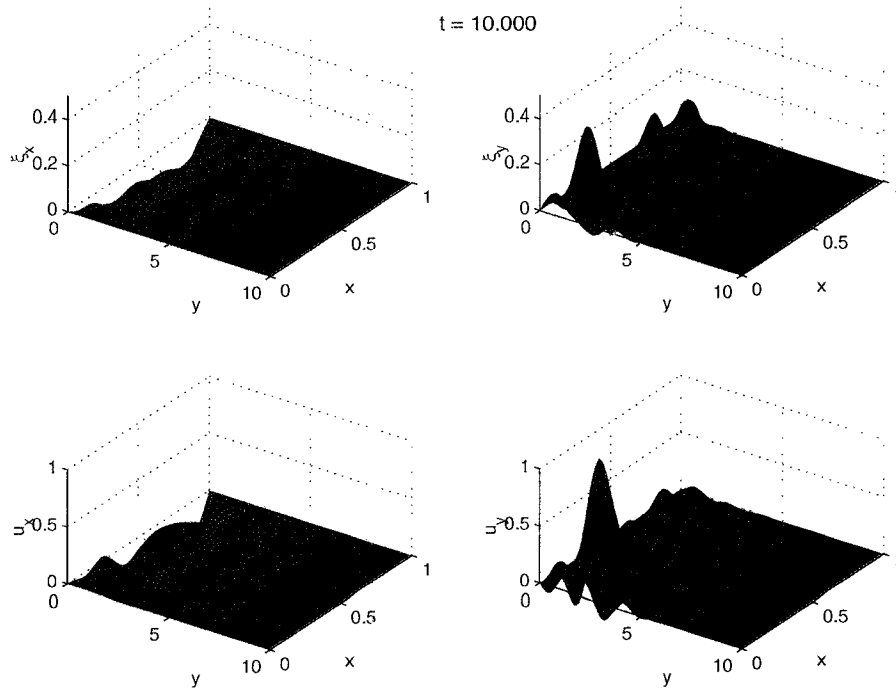
Figure 3.5: Velocity and displacement of the plasma at $t = 10$. The resonance has just appeared.
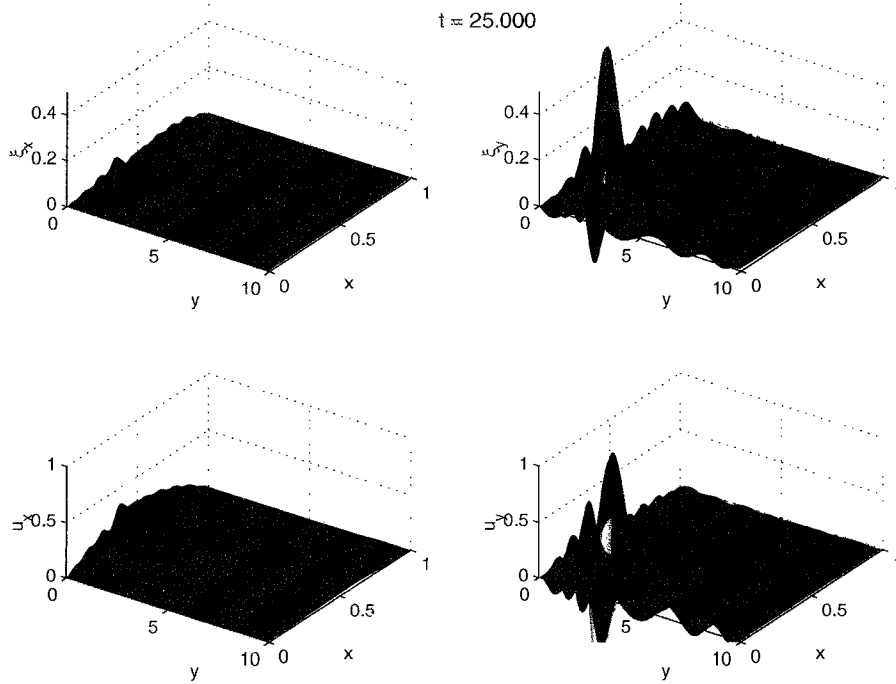

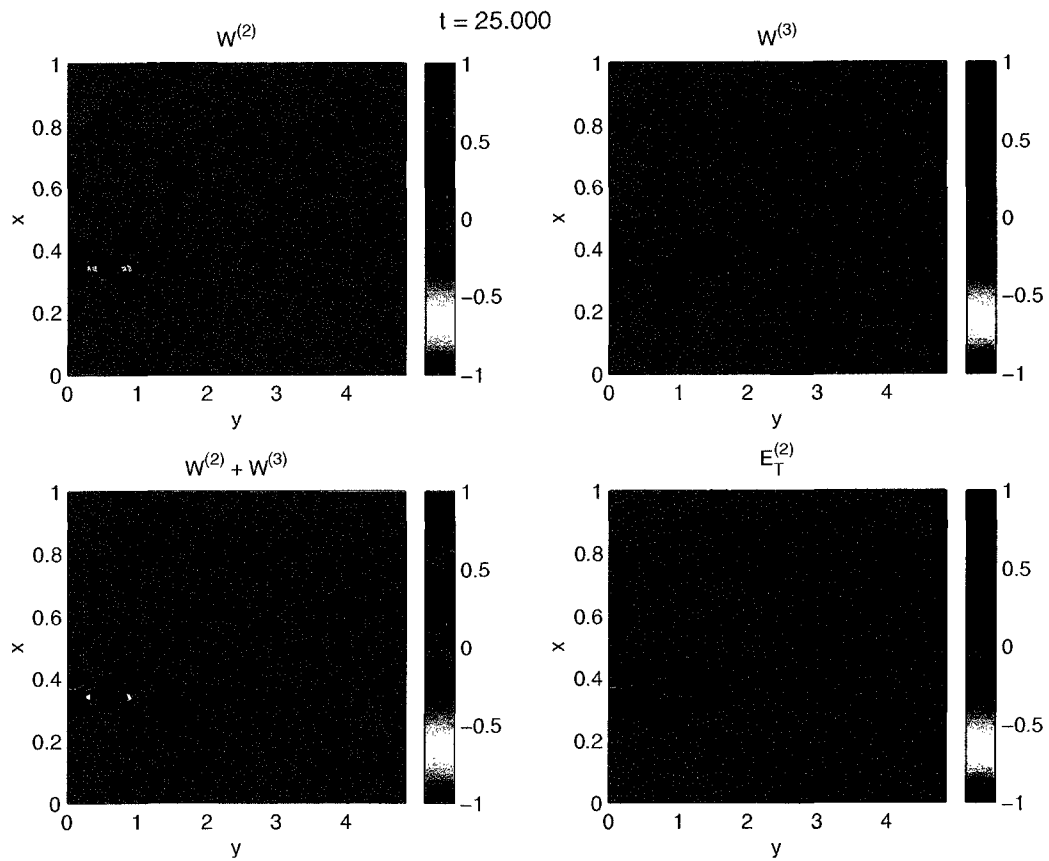Figure 3.6: Velocity and displacement of the plasma at $t = 25$.

42

Figure 3.7: Maps of the plasma energy density at $t = 25$.
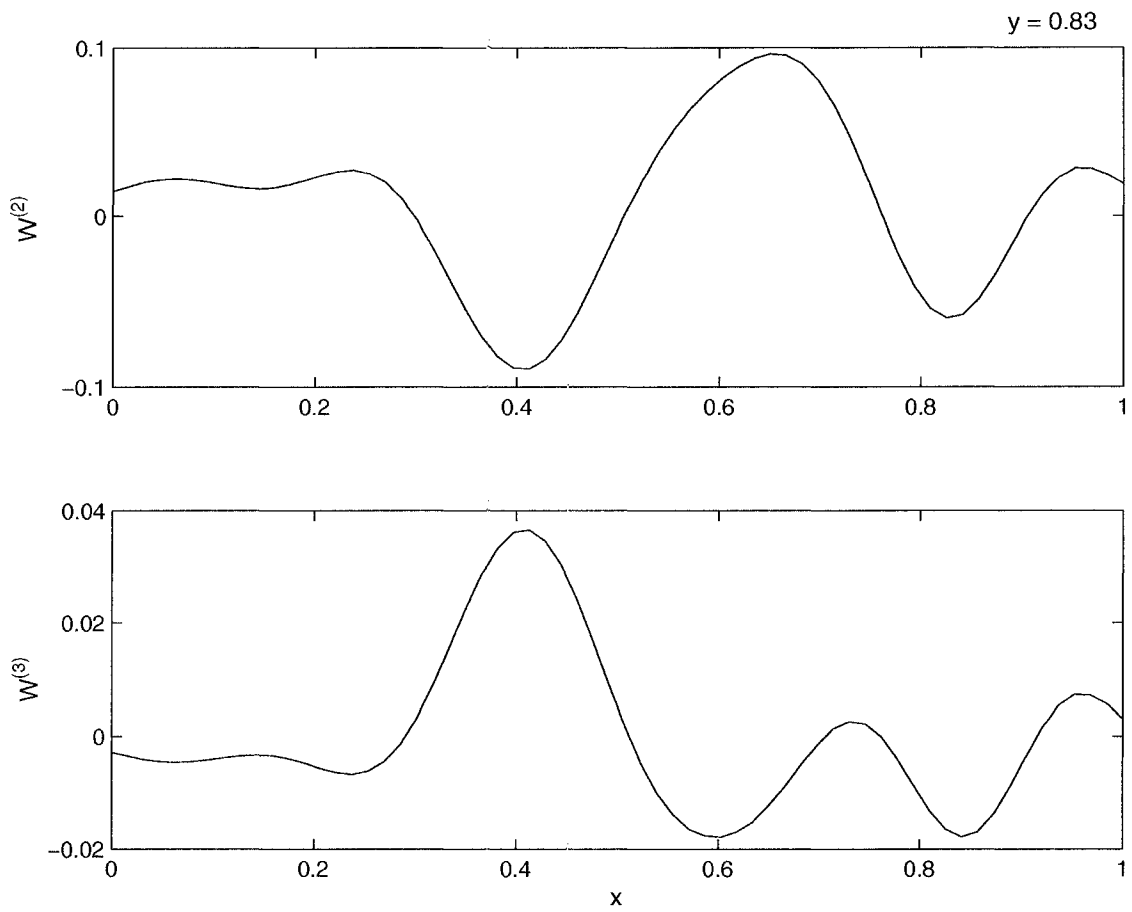
43

Figure 3.8: Profiles of the plasma energy density at $t = 5$ and $y = 0.83$. The coarseness is caused by the omission of the grid points in the plot.
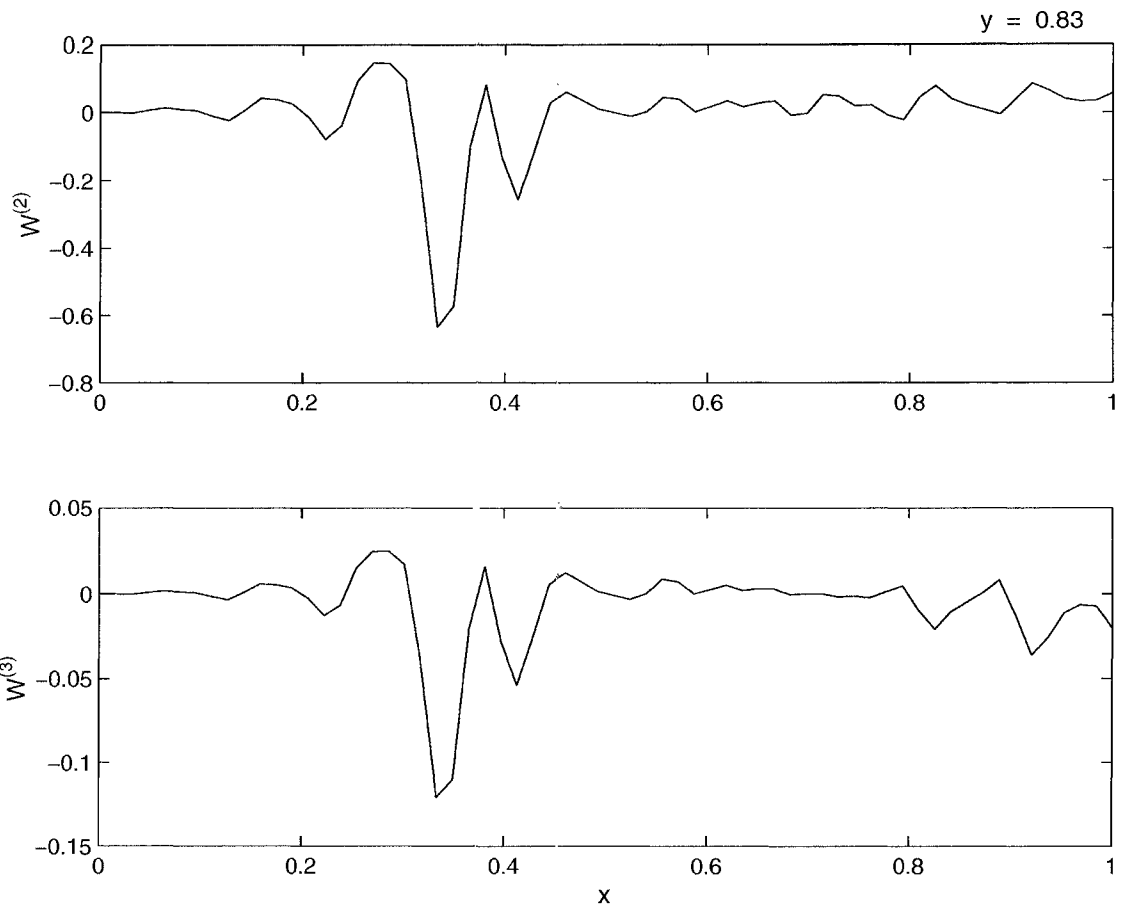
44

Figure 3.9: Profiles of the plasma energy density at $t = 25$ and $y = 0.83$. The coarseness is caused by the omission of the grid points in the plot.

45

3.3 Plasma in a Curvilinear Magnetic Field: Curvature-Gradient Instability in Stretched Field Line Topology

Though box models are a useful simplification for many physical systems on a local scale, to investigate plasma instabilities in realistic configurations, the modeling of a plasma in curvilinear coordinates is needed. This is mainly because many interesting features of the plasma behavior, for instance ballooning modes, need curved magnetic field lines to occur in the absence of gravity. Here we present an example of the instability investigation in a curvilinear magnetic field. Since our focus is primarily magnetospheric instabilities, we limited ourselves to a stretched magnetic field line configuration, similar to the one during substorm growth phase in the near Earth magnetotail.

3.3.1 Basic Equations

The MHD wave equation (2.50) we derived in Chapter 2 has already been written in a form that works in any geometry and in any coordinate system. For modeling purposes we used coordinates (x_1, x_2, x_3), such that the coordinate x_1 is directed along field lines, the coordinate x_2 is in the direction of the radius of curvature, and the coordinate x_3 is in the azimuthal direction (see Fig. 3.10). If the coordinate system (x_1, x_2, x_3) is not normalized (metric tensor differs from $\mathrm{diag}(1,1,1)$), we will denote such a coordinate system with bar over the letters $(\bar{x}_1, \bar{x}_2, \bar{x}_3)$. Also, in magnetospheric physics, especially in dipolar coordinates, or coordinates close to dipolar, a notation (μ, ν, ϕ) can be used instead of (x_1, x_2, x_3).
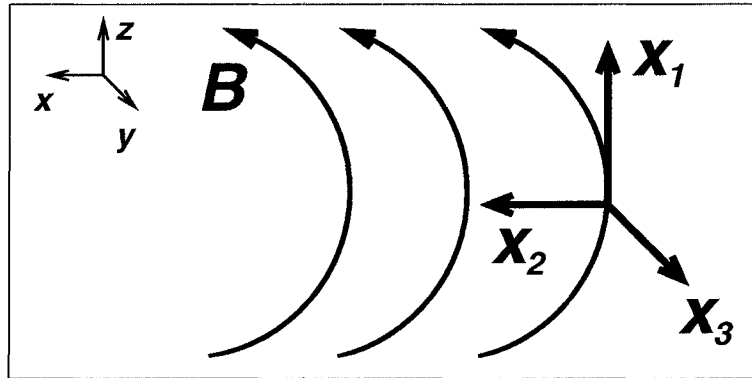

Figure 3.10: Sketch of curvilinear coordinates for the magnetospheric setting.

46

In this coordinate system equation (2.50) can be written for a cold plasma in the form

$$\rho \partial_{tt} \bar{\xi}_1 = 0, \tag{3.12}$$

$$\rho \partial_{tt} \bar{\xi}_2 = \frac{\bar{B}}{g_{22}} \partial_2 \left(\sqrt{g} \bar{B} (\partial_2 \bar{\xi}_2 + \partial_3 \bar{\xi}_3) \right) + \frac{\bar{B}}{g_{22}} \partial_1 (g_{22} \bar{B} \partial_1 \bar{\xi}_2), \tag{3.13}$$

$$\rho \partial_{tt} \bar{\xi}_3 = \frac{\bar{B}}{g_{33}} \partial_3 \left(\sqrt{g} \bar{B} (\partial_2 \bar{\xi}_2 + \partial_3 \bar{\xi}_3) \right) + \frac{\bar{B}}{g_{33}} \partial_1 (g_{33} \bar{B} \partial_1 \bar{\xi}_3), \tag{3.14}$$

where g_{ij} is metric tensor of the orthogonal coordinate system $(\bar{x}_1, \bar{x}_2, \bar{x}_3)$, and $g = \det(g_{ij})$. However, for computational purposes it is more effective to work in normalized coordinates instead. This is because the ambient quantities in orthonormal coordinates, corresponding to their counterparts in a orthogonal system, are $X_i^{(norm)} = h_i \bar{X}_i$, where the Lammé coeficients are given by the metric tensor in the coordinate basis $(\bar{x}_1, \bar{x}_2, \bar{x}_3)$, $g_{ij} = \text{diag}(h_1^2, h_2^2, h_3^2)$, and therefore have much smaller gradients close to the boundary. In these normalized basis (x_1, x_2, x_3), equations (3.12) to (3.14) have the form

$$\rho \partial_{tt} \xi_1 = 0, \tag{3.15}$$

$$\rho \partial_{tt} \xi_2 = \frac{B}{h_1 h_2} \left[\partial_2 (\partial_2 B h_3 \xi_2 + \partial_3 B h_2 \xi_3) + \partial_1 \left(\frac{h_2}{h_1 h_3} \partial_1 B h_3 \xi_2 \right) \right], \tag{3.16}$$

$$\rho \partial_{tt} \xi_3 = \frac{B}{h_1 h_3} \left[\partial_3 (\partial_2 B h_3 \xi_2 + \partial_3 B h_2 \xi_3) + \partial_1 \left(\frac{h_3}{h_1 h_2} \partial_1 B h_2 \xi_3 \right) \right]. \tag{3.17}$$

This result is consistent in a cold plasma approximation with the expression obtained by *Voronkov* [1998] for a dipolar field. However, equations (3.15) to (3.17) are valid in any plasma system where coordinates are defined consistently with Fig. 3.10. The coefficients h_1, h_2 and h_3 contain the information of the geometry of the system.

We limited ourselves to a 2-dimensional problem in the xz plane. The grid we use is uniform in spherical coordinates r and θ. We then transformed this grid into coordinates x_1 and x_2. Figures 3.11 and 3.12 show the grid used in our model, and the comparison between dipolar coordinates and the stretched topology we used, respectively. Since this system contains free energy in a form of gradients and curvature of the magnetic field, it is possible for this system to be unstable.

At first we made several runs for a dipolar magnetic field where we know that the system must be stable since, for cold plasma, a dipolar field is the lowest energy state and therefore it does not contain any free energy. Indeed we observed consistently stable solutions for different initial conditions.

Then we changed topology to a stretched magnetic field lines similar to the magneto-spheric configuration during the substorm growth phase. Even in the simple case of cold
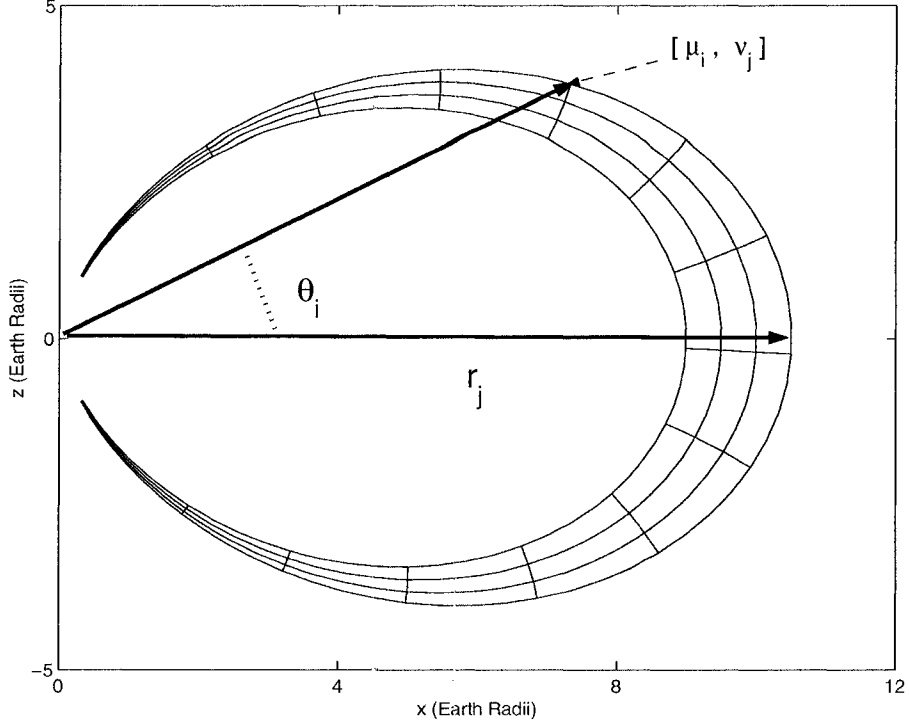
47

Figure 3.11: Grid used in the curvilinear coordinates.

plasma there is a free energy stored in the curvature of the field lines, and in currents [*Ortolani and Schnack*, 1993].

Voronkov et. al. [2000] discuss the stability of the equatorial region in the stretched field topology with respect to the ballooning modes. Their expression for the ballooning mode frequency in the equatorial plane simplifies for a cold plasma to

$$W^2 = -\frac{2V_A^2}{R^2}\left(\frac{B'R}{B} + 1\right),$$ (3.18)

where V_A is Alfvén velocity, B is the magnitude of magnetic field, R is the radius of curvature of field lines, and B' is the radial derivative of magnetic field. It is obvious that this result allows the growth of a linear instability, even for cold plasmas.

3.3.2 Initial Configuration

To specify the initial equilibrium magnetic field we used the definition of the normalized coordinate along field lines $x_1 = B/B$. Since we know that the magnetic field must be by definition of x_1 along this coordinate, and the relation between normalized base vectors and coordinate basis, where e_1 corresponds to $\partial_\parallel$ and $\bar{B}^i = M(= const)$, $x^i = h_i \bar{x}^i$, the magnetic field can be simply defined as $B_1 = M/h_1$ where M is the magnetic moment.
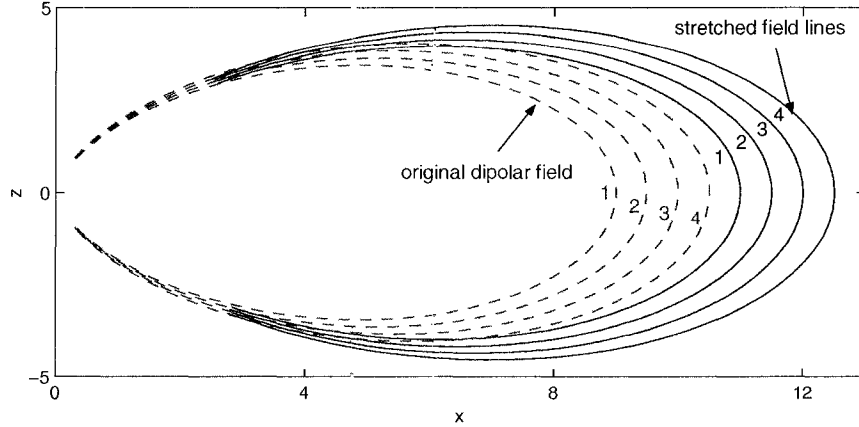
48

Figure 3.12: Comparison between dipolar topology and the stretched field line topology we used. Numbers denote corresponding field lines.

However, to satisfy condition $\nabla \cdot \boldsymbol{B} = 0$ components of the metric tensor must satisfy the relation $h_1 = h_2 h_3$. An example of this type of coordinate system is dipolar coordinates.

At first we have performed several test runs with a zero azimuthal wave number. In this instance wave modes are not coupled and the ballooning mode cannot evolve. Indeed, we observed stable behavior of the system, with the fast evolution of the eigenmodes from the near-eigenmode initial impulse. These runs served to verify if there are no numerical instabilities introduced into the system by the boundary conditions.

Then we allowed non-zero azimuthal wave number k_ϕ, in other words we allowed coupling between different modes. We introduced an initial compressional wave into the system in the form of a narrow Gaussian peak. This mode was coupled to the azimuthal component of the displacement through non-zero k_ϕ.

The ionospheric boundary is assumed to be reflective, with ξ_i, $u_i = 0$, $i = 1, 2, 3$, and is localized at $r = 4$ to avoid steep gradients in ambient quantities for lower r. At the equator the field lines ranged from $r = 11$ to $r = 13$. Across field lines we assumed an open boundary ($\xi_{i,j} = 0$, $u_{i,j} = 0$, $i, j = 1, 2, 3$ to allow for wave propagation in this direction. We used a grid 256 (along field lines) $\times$ 128 (across field lines). This spatial resolution was the same as we used for the dipolar model and the stretched magnetic field topology with zero azimuthal wave number. The time step $dt = 0.00001$ and we ran for $0 < t < 1000$ which allowed sufficient time for possible interesting features to develop. The ambient magnetic field and plasma density are defined as $B = M/h_1$, where $M = 0.05$, and $\rho = \rho_0 / \sin^8 \theta$, with $\rho_0 = 10^{-5}$. Figure 3.13 shows the ambient magnetic field and plasma density, and Figure 3.14 shows the Alfvén velocity dependence. The azimuthal wave number was $k_\phi = 2$.
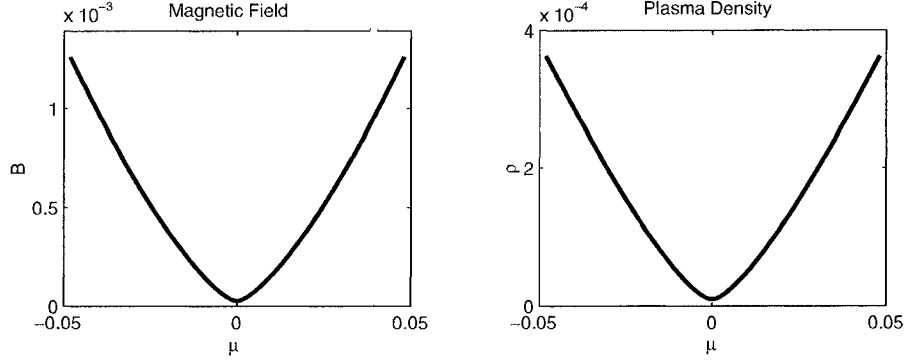
49

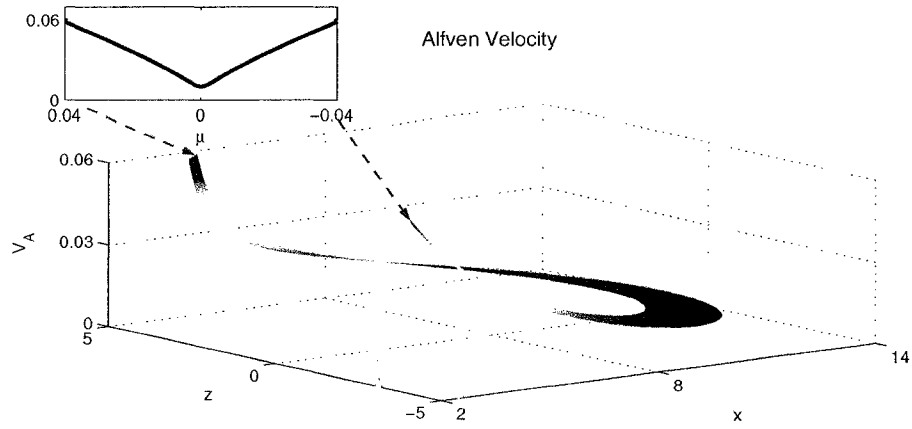Figure 3.13: Ambient stretched magnetic field and plasma density.

Figure 3.14: Alfvén velocity dependence in a stretched field line topology.

The initial displacement and velocity were

$$\xi_{i0} \;=\; 0, \qquad i = 1, 2, 3, \tag{3.19}$$

$$u_{i0} \;=\; 0, \qquad i = 1, 3, \tag{3.20}$$

$$u_{20} \;=\; \Lambda \exp\left(-\,\frac{(r - r_0)^2}{\delta^2} \right) \exp\left(-\,\frac{(\theta - \theta_0)^2}{\sigma^2} \right), \tag{3.21}$$

where $\Lambda = 0.0005$, $r_0 = 12$, $\delta = 0.2$, $\theta_0 = \pi/2$, and $\sigma = 0.015$. Figure 3.15 shows the initial velocity profile. This choice of initial velocity corresponds to introducing an initial compressional wave into the system.

Dynamics of the System

Due to the presence of a non-zero azimuthal wave-number the initial impulse generates a shear Alfvén wave along field lines. This coupling sends an impulse from the equatorial region toward the ionosphere. Figures 3.16 to 3.21 show the overall behavior of the plasma
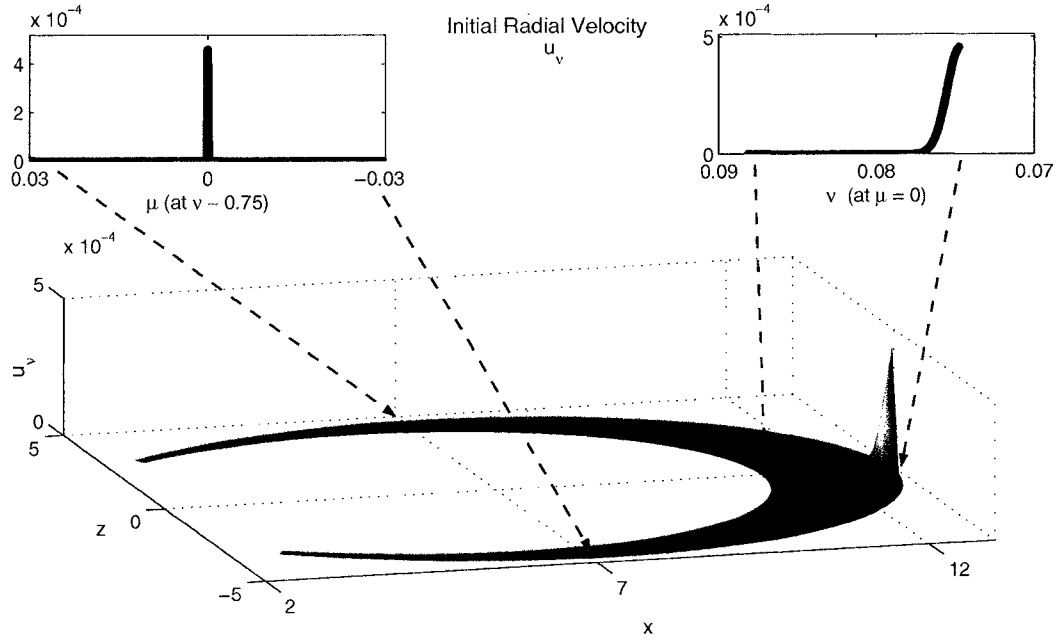
50

Figure 3.15: Initial radial impulse introduced into the system. Due to a non-zero azimuthal wave number this impulse generated shear Alfvén waves.

displacement and velocity at times $t = 200$, $t = 600$, and $t = 1000$. We can clearly distinguish propagation of the impulse toward the ionosphere, and profiles in the equatorial plane exhibit earthward drift of the plasma waves.

Also, we can observe the exponential growth of the amplitude of both, compressional, and shear Alfvén wave, in other words we observe a linear curvature-gradient instability. Before the wave packet reaches the ionospheric boundary, the exponential growth saturates and the system goes eventually into an oscillatory mode. Time evolution of the magnitude of the plasma displacement in the equatorial plane is illustrated in Fig. 3.22. The energy source for this system is in the stretching, and therefore changing curvature, of the field lines, and in gradients of currents that are present due to coupling between modes.

Using the energy analysis, discussed in Chapter 2, this behavior can be explained very easily, in an analogy with a mechanical system. Fig. 3.23 illustrates the dynamics of an object in a potential field of the form $U = \alpha x^2 + \beta x^3$ (the non-linear slide in Fig. 3.24). We can see the initial exponential growth that eventually saturates (slows down into virtually zero), but as soon as the object passes a threshold, its behavior becomes singular. However, if we omitted the cubic part of the energy (quadratic well in Fig. 3.24) from the description of the system, the singular phase would not occur, instead, after the initial exponential phase, the object would start to oscillate in the potential well between the two points with

51

the highest altitude it reached during the initial stage.

Similarly, the plasma waves exhibit initial exponential growth which corresponds to a ball rolling down the hill in the quadratic well. As it reaches the top of its trajectory, it slows down, and then starts to oscillate. Also the amplitude of the ballooning mode evolves through the exponential growth and saturation (growth slows down to zero) into oscillations with the amplitude equal to the maximum amplitude during the instability. However, as we shall see from the analysis of the energy density, the real plasma behavior in this topology corresponds to a non-linear phase, and the short period of zero growth would be an onset of singular growth.

Analysis of the Energy

The linear approximation used to derive equation of motion (2.50) that we have used in modeling the dynamics of the system assumes a negligible cubic term in the expansion of the energy. Calculation of the energy density reveals that this term becomes important during the linear stage of instability. Neglecting this term causes the occurrence of the oscillatory mode instead of the nonlinear instability in the system. At this point the linear approximation is no longer correct.

Figures 3.25 to 3.27 show maps of the energy density at times $t = 200$, $t = 600$, and $t = 1000$. The small figures are energy density profiles in the equatorial plane. Since the energy density is a function of the gradient of displacement, the original double peak shape along the field lines is a result of the original impulse introduced into the system. These figures illustrate a steady increase in the energy density due to the linear instability in the plasma.

Figures 3.28 and 3.29 show the time evolution of the energy densities in the equatorial plane in normal and logarithmic scales. Here we can observe that during the exponential growth stage the second order energy dominates. The beginning of the saturation stage corresponds to time when the second and the third order terms in energy become comparable, and thus the linear approximation ceases to be adequate. When the third order term starts to dominate we are looking at the onset of explosive behavior and the linear treatment is fully inadequate.
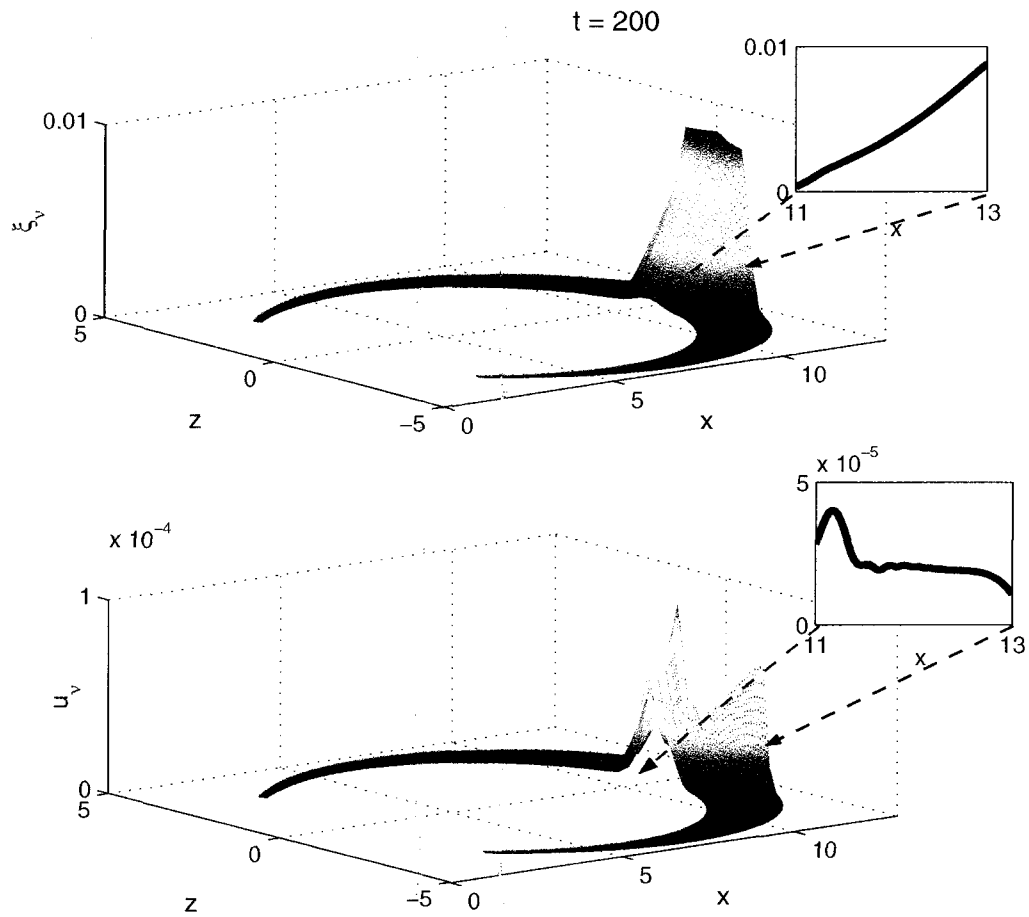
52

Figure 3.16: Plasma displacement and velocity perpendicular to field lines at $t = 200$.
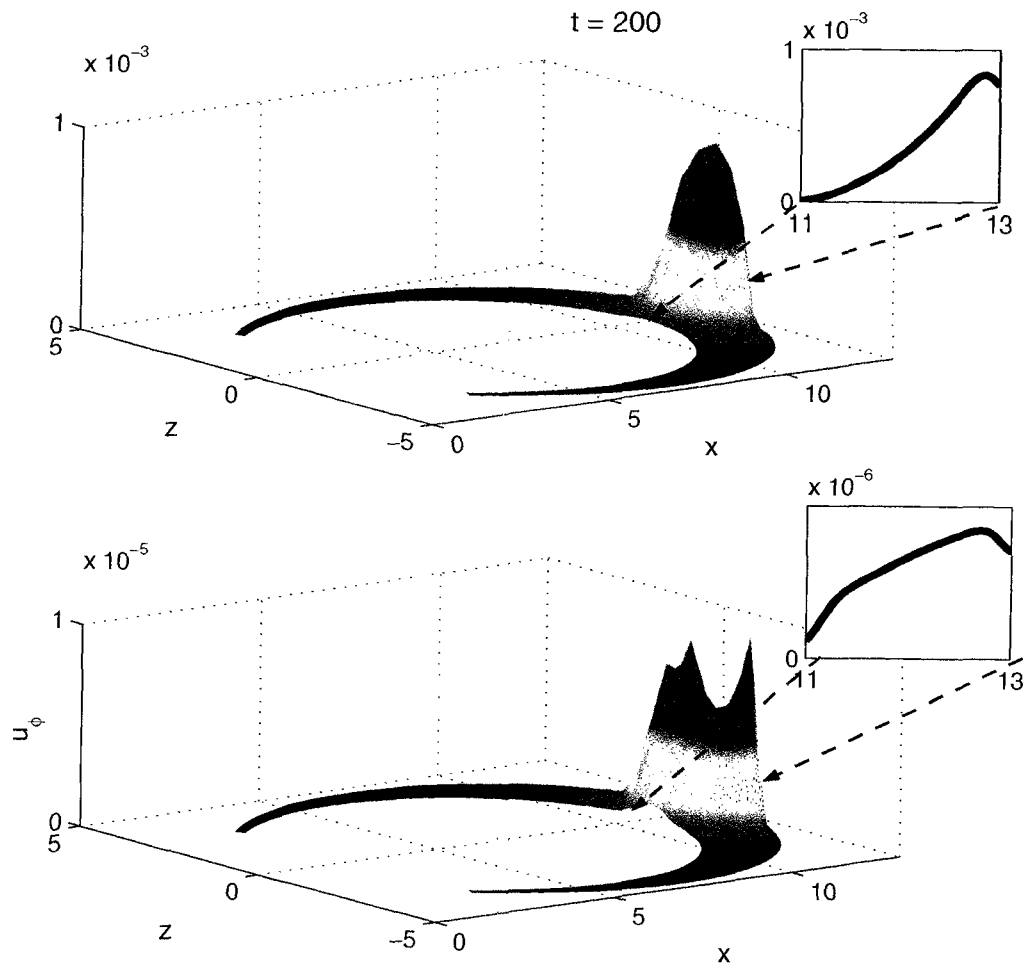
Figure 3.17: Azimuthal component of the plasma displacement and velocity at $t = 200$.
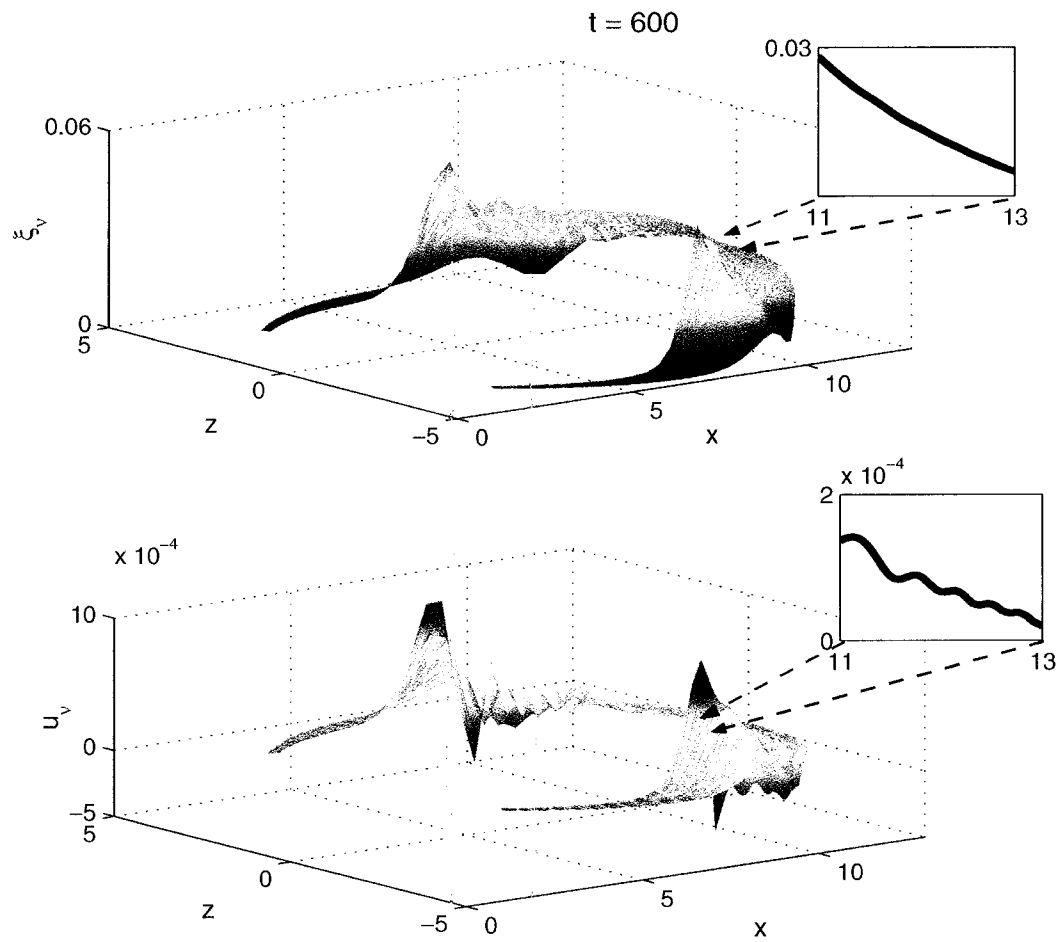
Figure 3.18: Plasma displacement and velocity perpendicular to field lines at $t = 600$.
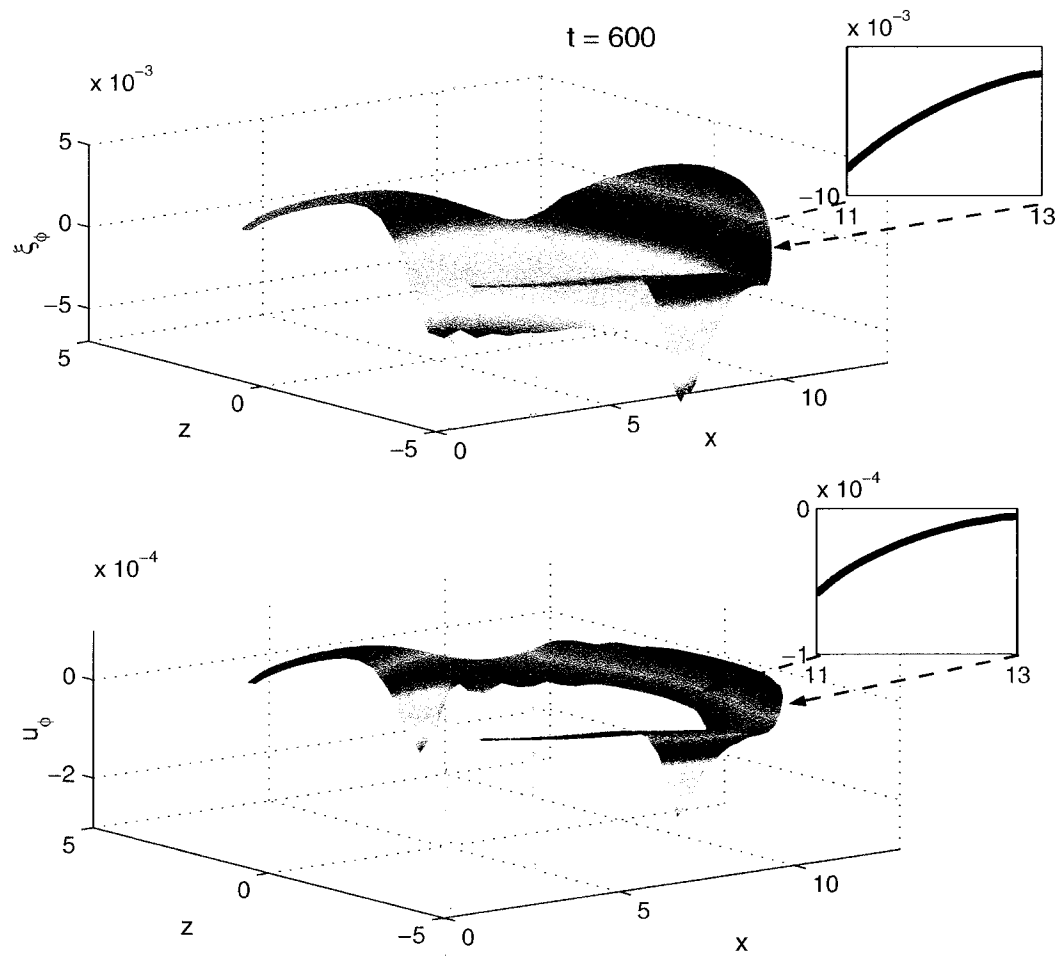
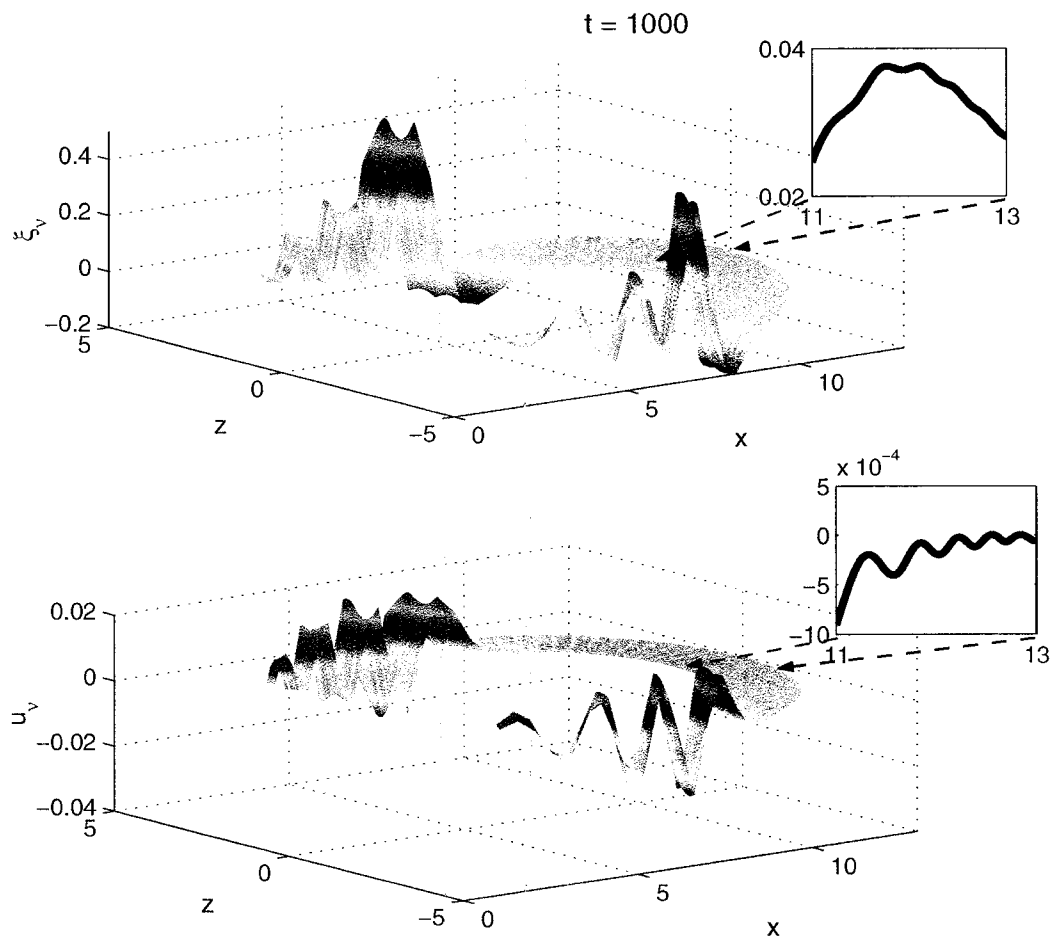Figure 3.19: Azimuthal component of the plasma displacement and velocity at $t = 600$.

56

Figure 3.20: Plasma displacement and velocity perpendicular to field lines at $t = 1000$.
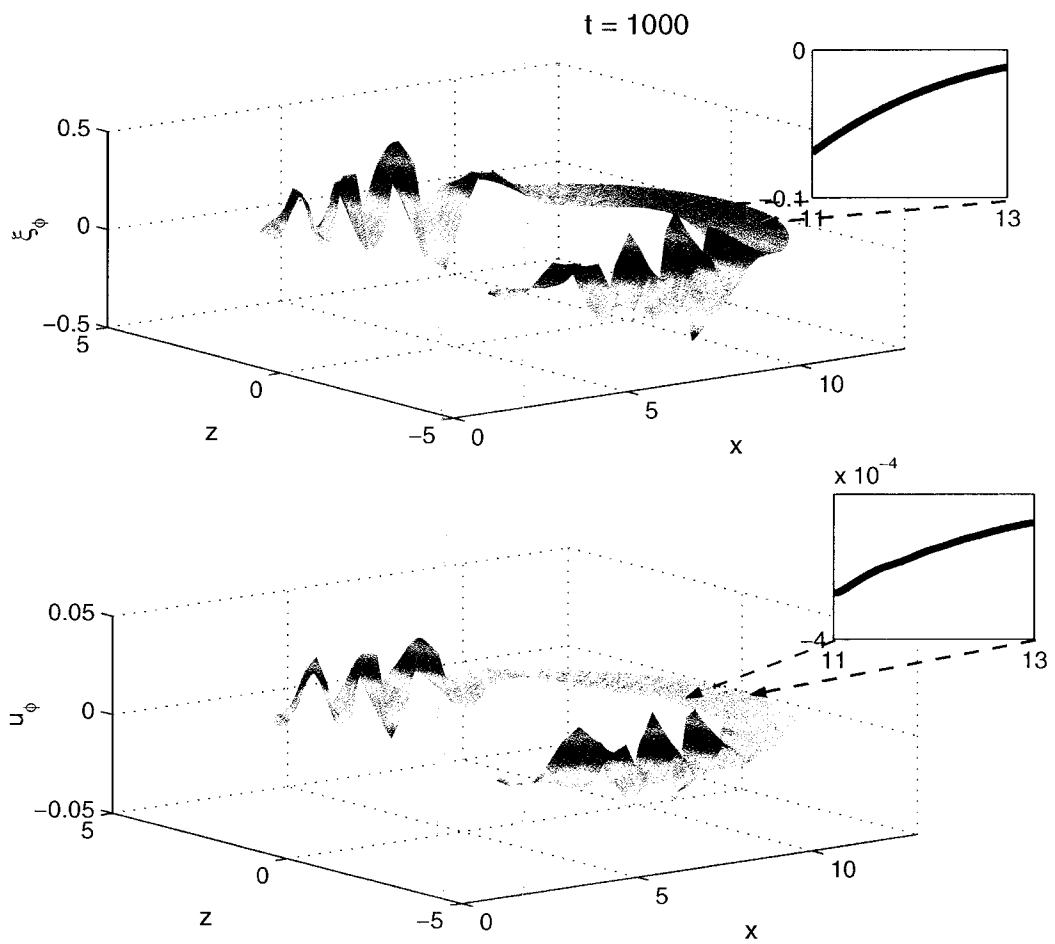
57

Figure 3.21: Azimuthal component of the plasma displacement and velocity at $t = 1000$.

58

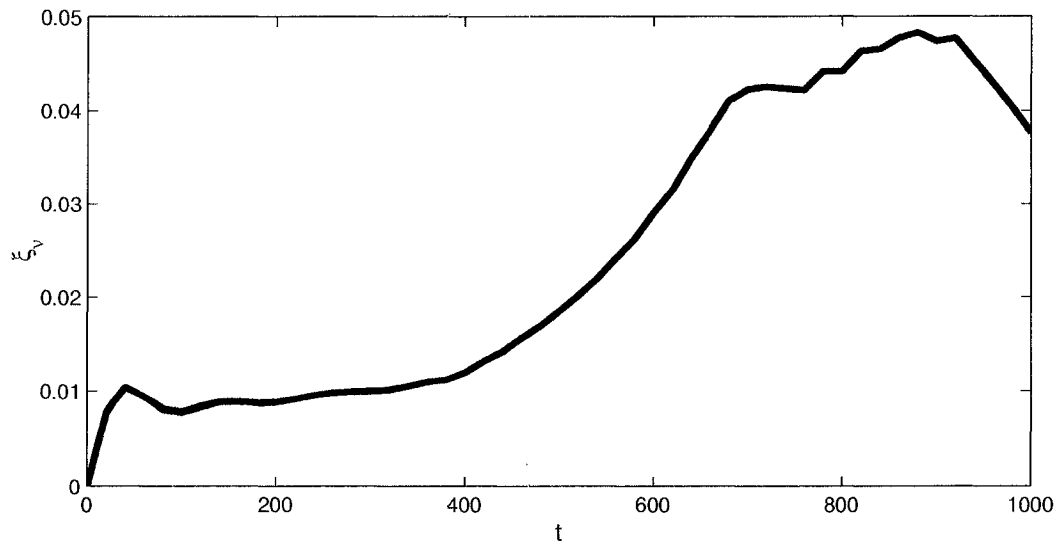Figure 3.22: Time evolution of the magnitude of the plasma displacement at the equator.
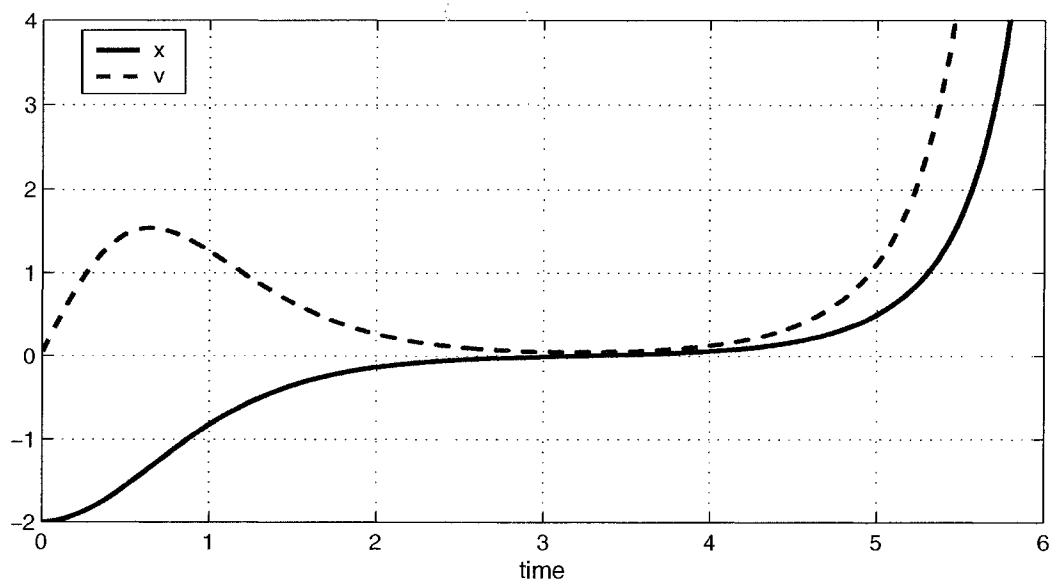
Figure 3.23: Dynamic of a mechanical system with energy $-2x^2 - x^3$.

59
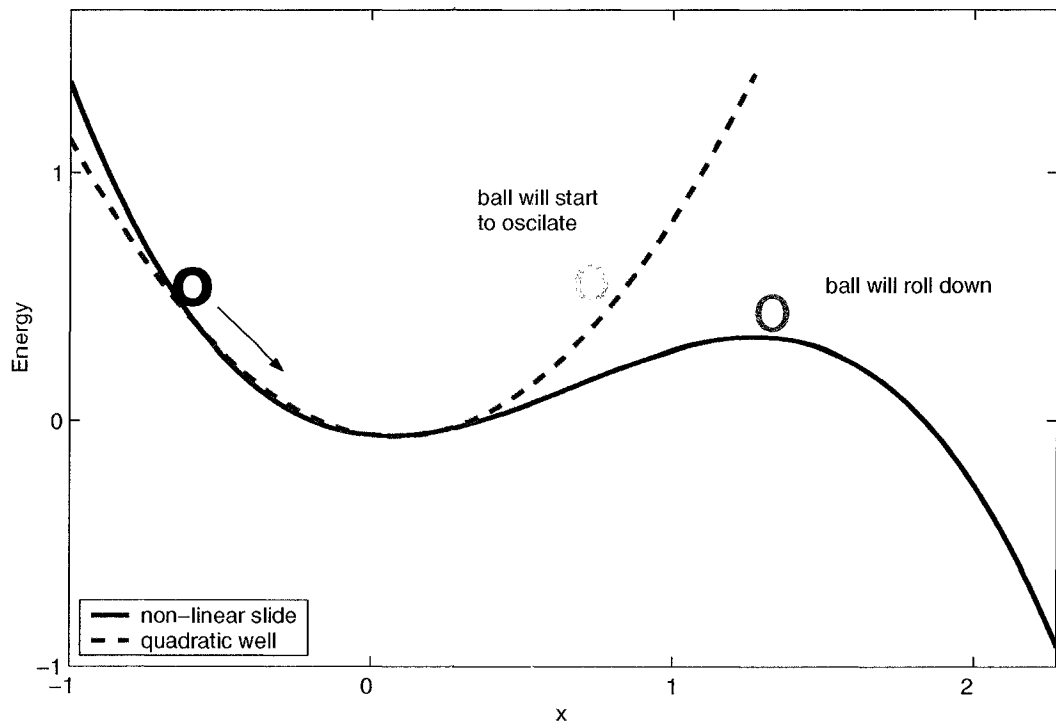
Figure 3.24: Comparison between the non-linear slide (potential energy is a combination of quadratic and cubic parts), and the quadratic well.

60
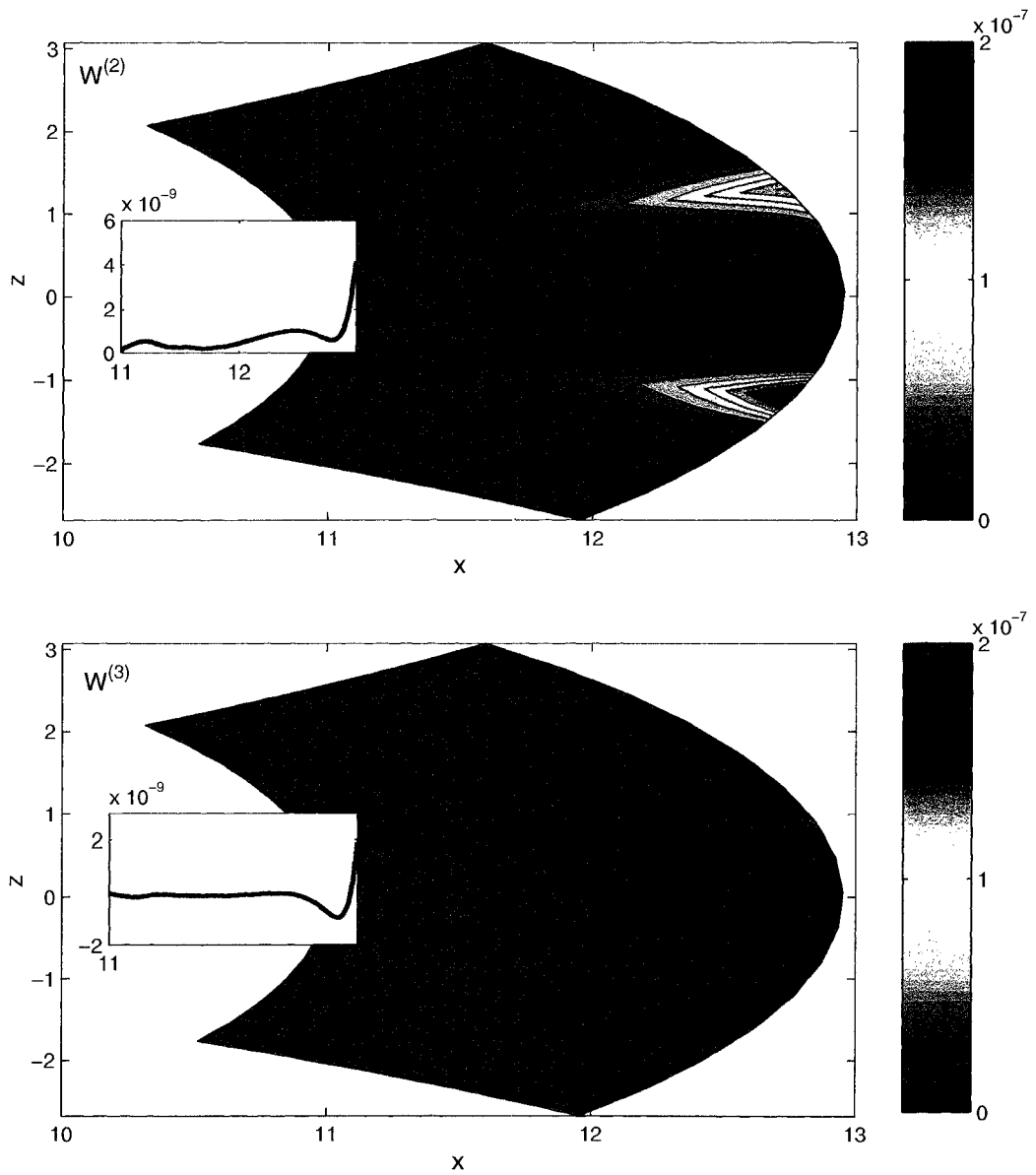
Figure 3.25: Energy density at time $t = 200$. The second order energy dominates the system.
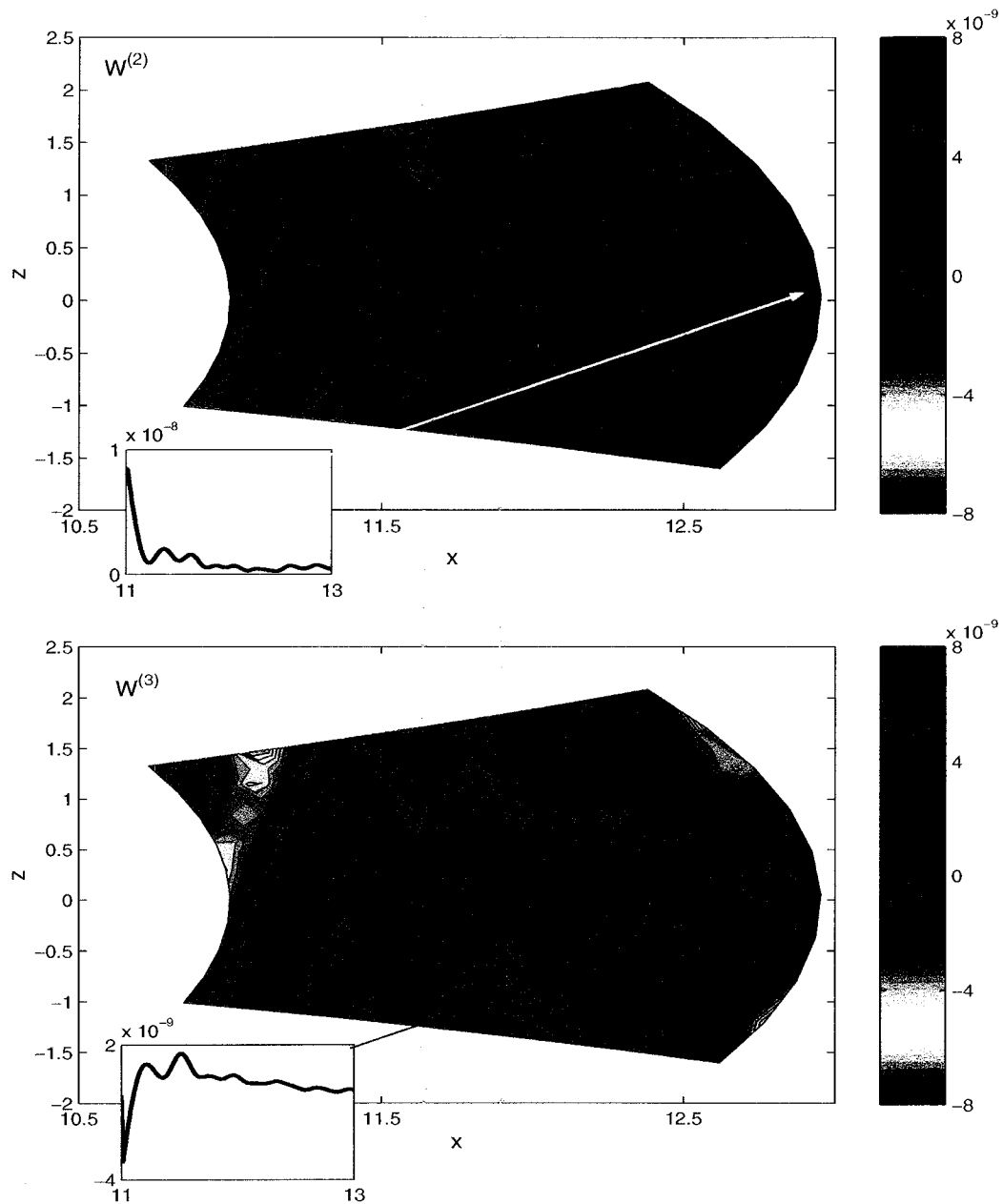
Figure 3.26: Energy density at time $t = 600$. The second and the third order terms are comparable.

62

Figure 3.27: Energy density at time $t = 1000$. Now the third order energy dominates and the linear description is no more valid.

63

Figure 3.28: Time evolution of the energy density in the equatorial plane.

Figure 3.29: Time evolution of the energy density in the equatorial plane, logarithmic scale.

64

3.3.3 Discussion

The situation with a stretched, curved magnetic field topology proved to be an interesting example of an explosive instability evolving from an initially linear instability.
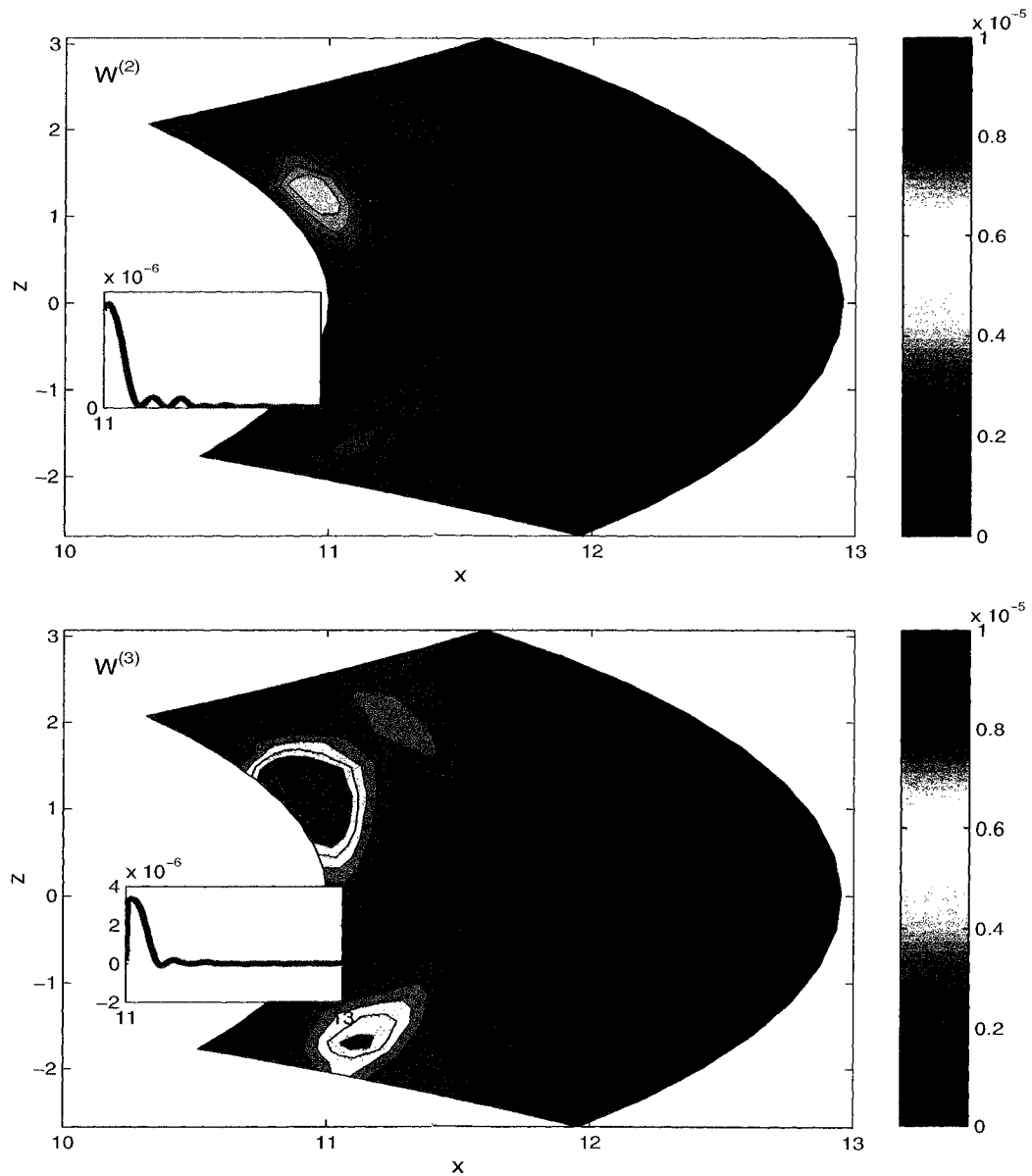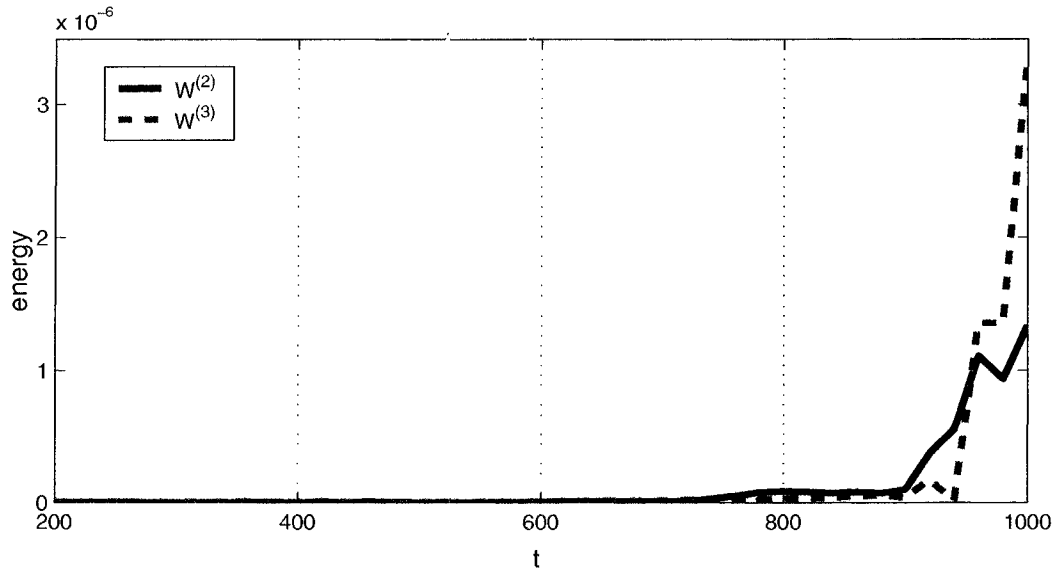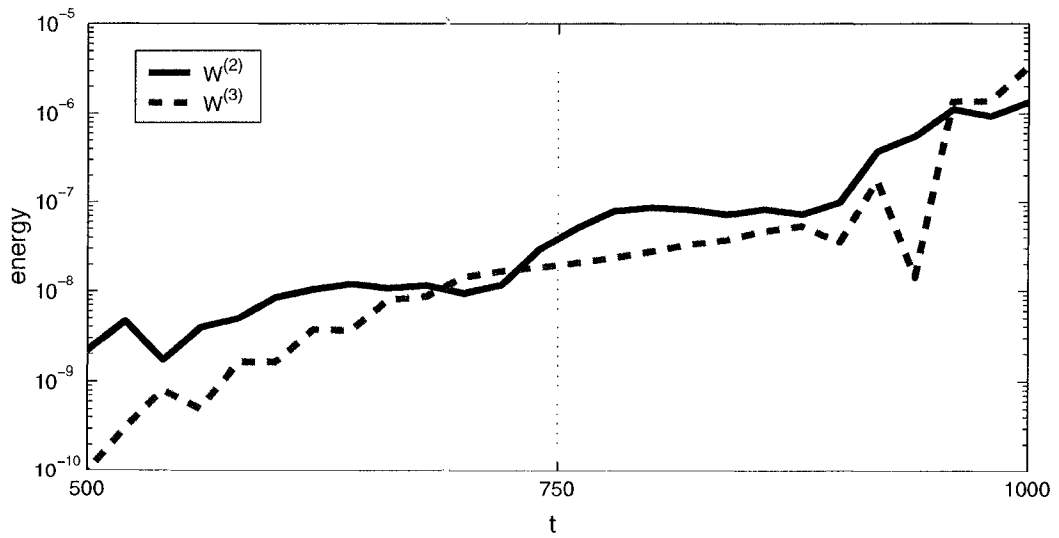
We have compared our results with the results of the non-linear numerical modeling of ideal MHD using an ADI code [*Voronkov et. al.*, 2000]. The system dynamics obtained from the nonlinear simulation is in Fig. 3.30 which shows a time dependence of the maximum of vorticity. Originally the system is in the equilibrium state that is disturbed by a small perturbation of the radial component of the velocity. This gives a start of the linear stage of the instability. Saturation occurs due to magnetic field compression that tends to bring the system into an oscillatory mode. However at this stage, the nonlinear terms begin to play a dominant role, providing onset of the explosive stage. This is in a good qualitative agreement with the results obtained from our model.

It is also interesting to compare our results with observations. It appears that the intensification of an auroral arc starts with a linear stage (the intensity of the arc grows exponentially), and eventually it evolves into an explosive disruption of the arc (breakup) [*Voronkov et. al.*, 2002]. Again, this is in a qualitative agreement with the results obtained from our model, which allow evolution of explosive behavior from an initial linear instability.
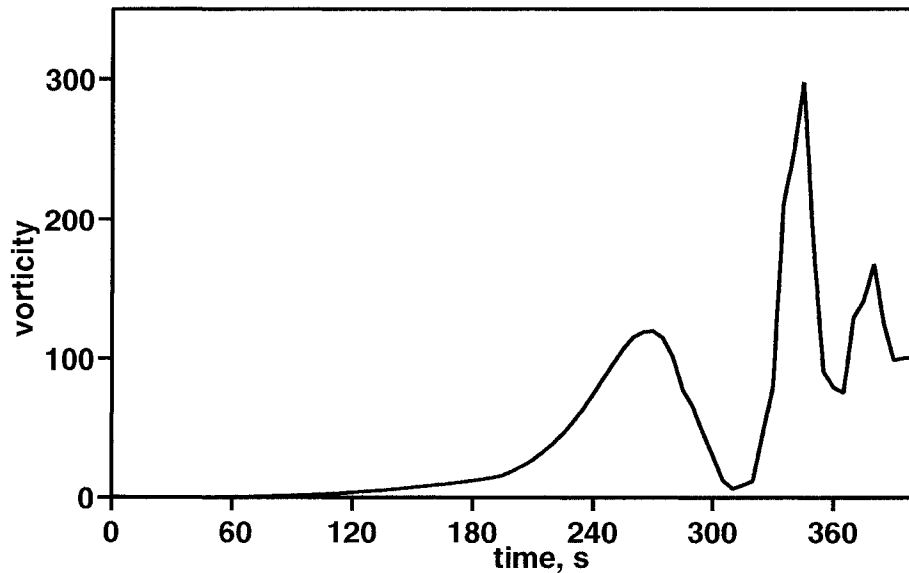
Figure 3.30: The time evolution of the plasma from the ADI code [Voronkov et al., 2000].

To conclude, our model provided us with results which suggest that in a stretched field line topology it is possible to trigger explosively unstable behavior by a short phase of initial linear instability growth. This result is in a good agreement with both observations and non-linear MHD modeling, for similar plasma configurations.

This agreement between our method and the results of non-linear numerical modeling and observational data confirms the usefulness and robustness of our method for non-trivial plasma configuration. The results we were able to obtain are encouraging for the future study of explosive phases of magnetospheric substorms, and also for the investigation of stability of toroidal plasmas. It appears that ballooning modes might be responsible for triggering the explosive stage of the substorm. However, further studies including models with more realistic, data based hot plasma configurations are needed for more reliable results.

Chapter 4

Conclusion

A description of an explosive behavior of magnetized plasmas is probably one of the grand challenges of modern physics. Despite the very common occurrence of this phenomenon, we have very limited understanding of the underlying processes due in part to very short time-scales and complicated non-linear equations needed to describe these phenomena. Also, because of the short time-scales involved, kinetic theory needs to be included in the full description of explosive instabilities, since fluid description requires low-frequency processes $(\omega \ll \Omega_{Gion})$. However, a fluid theory can often be a reasonable description for various physical systems during times preceding an instability (For detailed treatment of the applicability of MHD to magnetospheric problems (collisionless plasmas) see [*Chew et al*, 1956]).

We have presented a method for the investigation of the possibility that a magnetized plasma configuration can evolve into an explosively unstable state. This method is based on a variational approach and eliminates the need to solve non-linear equations. The variational approach is combined with a geometrical treatment of plasma perturbations, leading to considerable simplification in the governing equations. Clearly, the variational approach is a very promising tool in dealing with plasma instabilities (see for instance [*Pfirsch and Sudan*, 1993] and [*Ilginois and Pastukhov*, 2000]). The application of geometry in perturbation calculations significantly simplifies the algebra and also leads to results that are in a very compact form, and immediately suitable for further calculations.

Our method is also based on an analogy with classical mechanics, and utilizes the principle that equivalent equations must yield equivalent solutions. Mechanical systems are much more intuitive and are also well understood for many non-linear models. In mechanics, if the potential energy of the system has a cubic dependence, the corresponding momentum equation has a singular, explosive solution. In analogy with this result, we assume that plasma systems with dominant third order potential energy will be explosively unstable.

67

We have demonstrated this method for an ideal MHD system, which is a simple, yet rather rich approximation of a plasma behavior leading to an excellent tool for the testing of new theoretical approaches. However, our method will work for any description of plasmas, where we can define a Lagrangian of the system.

After building a theoretical framework for ideal MHD we applied this theory to two different types of plasma configurations. In one of them, the magnetic field was rectilinear and in the other the magnetic field topology was curvilinear. To avoid problems with the initial equilibrium we considered only cold plasma approximations, for which the equilibrium was easy to find. Our purpose was to show that this method is relatively simple and quite practical, and can be applied to explosive instability investigations in realistic plasma configurations, including the stretched field topology of the Earth's magnetotail.

We obtained both negative and positive results for different systems. Systems with rectilinear and dipolar fields were stable. This is a reasonable result, since in a rectilinear field ballooning modes cannot evolve due to the absence of curvature forces, and a dipolar field is a stable configuration, since it is the lowest energy state. Nevertheless, these examples serve to illustrate simple applications of our method and indicate that the method leads to accurate results.

The stretched topology model led to very interesting results. A very small initial perturbation initiated a linear curvature-gradient instability that quickly evolved into an explosively unstable phase over an interval of about 1000 dimensionless time units, corresponding to few minutes of real time. These computations were performed for a cold plasma, and we assume that the presence of a thermal pressure gradient could enhance this instability.

The time-scale of this instability corresponds to the timescales for the onset of the substorm expansive phase. This would leave the possibility that the onset of the expansion phase of the substorm could be caused by small fluctuations in a plasma evolving through a short linear phase to an explosive phase. This would also limit the need for external trigger mechanism for substorm onset and would confirm that the processes beyond core crashes in toroidal plasmas and substorm onset are caused by the same type of generic plasma relaxation process [*Ortolani and Schnack*, 1993].

Future work in this area should involve the inclusion of a Hall term, which would make possible the consideration of reconnection processes (tearing mode), and the development of numerical models for tests for nonlinear instabilities in various plasma configurations, including systems with negative curvature and toroidal systems. The ability to detect unstable plasma configurations in advance would be a great asset in our struggle for the understanding of the fundamental processes in plasmas in a wide variety of areas.

68

Notation

L	Lagrangian
$\mathcal{L}$	Lagrangian density ($L = \int dV \mathcal{L}$)
$X^{(i)}$	i-th order quantity
$\hat{X}$	perturbed quantity X ($\hat{X} = X + \delta X$)
W	Potential energy density
B	ambient magnetic field
P	ambient pressure
ρ	plasma density
v	plasma velocity
γ	isotropic coefficient
ξ^i	plasma displacement
g_{ij}	metric tensor
g	$= \det(g_{ij})$
$\mathbf{1}$	unit matrix
ϵ_{ijk}	Levy - Civita symbol
δ^{ijk}_{lmn}	generalized Kronecker delta (product of δs antisymmetrized in all indices)
$a_{[ij]}$	antisymmetrization in i,j indices
$a_{,i}$	$= \partial_i a$
$a_i b^i$	$\equiv \sum_i a_i b^i$
a^i	vector
a_i	covector (object such that $a^i a_i$ is scalar)

69

Bibliography

[1] D.N. Baker, T.I. Pulkkinen, V. Angelopoulos, W. Baumjohann, and R.L. McPherron. The neutral line model of substorms: Past results and present view. *J. Geophys. Res.*, 101:12975, 1996.

[2] G.F. Chew, M.L. Goldberger, and F.E. Low. The boltzmann equation and the one-fluid hydromagnetic equations in the absence of particle collisions. *Proc. Roy. Soc. London*, 236A:112–118, 1956.

[3] S. C. Cowley and M. Artun. Explosive instabilities and detonation in magnetohydrodynamics. *Physics Reports*, 283:185–211, 1997.

[4] R.P. Feynman, R.B. Leighton, and M. Sands. *The Feynman lectures on physics, Vol. 2*. Addison-Wesley publishing company, 1977.

[5] H. Flanders. *Differential forms with application to the physical sciences*. Academic Press, New York - London, 1963.

[6] E. Friedrich, J. C. Samson, and I. Voronkov. Ground-based observations and plasma instabilities in auroral substorms. *Physics of Plasmas*, 8:1104–1110, 2001.

[7] E. Hameiri, P. Laurence, and M. Mond. The ballooning instabilities in space plasmas. *Jour. of Geophys. Res.*, 96:1513–1526, 1991.

[8] B. G. Harrold and J. C. Samson. Standing ULF modes of the magnetosphere: a theory. *Geoph. Res. Let.*, 19:1811–1814, 1992.

[9] O. A. Hurricane, B. H. Fong, and S. C. Cowley. Nonlinear magnetohydrodynamic detonation:part 1. *Phys. Plasmas*, 4:3565, 1997.

[10] V. I. Ilginois and V. P. Pastukhov. Variational approaches to the problem of plasma stability and of nonlinear plasma dynamics. *JETP Letters*, 72:530–540, 2000.

[11] S. I. Itoh, K. Itoh, H. Zushi, and A. Fukujama. Physics of collapse events in toroidal plasmas. *Plasma Phys. Control. Fusion*, 40:879–929, 1998.

[12] L.D. Landau and E.M Lifshitz. *Mechanics*. Butterworth-Heinemann, 3 edition, 1976.

[13] L.D. Landau and E.M Lifshitz. *Elektrodinamika Splosnych Sred*. Nauka, Moscow, 1992.

[14] W. W. Liu. Physics of the explosive growth phase: Ballooning instability revisited. *J. Geophys. Res.*, 102:4927–4932, 1997.

[15] S. Lundquist. On the stability of magneto-hydrostatic fields. *Phys. Rev.*, 83:307, 1951.

[16] D.R. Nicholson. *Introduction to plasma theory*. John Wiley & sons, 1983.

[17] S. Ohtani, K. Takahashi, L.J. Zanetti, T.A. Potemra, R.W. McEntire, and T. Iijima. Initial signatures of magnetic field and energetic particle fluxes at tail reconfiguration: Explosive growth phase. *Jour. of Geophys. Res.*, 97:19311, 1992.

[18] S.I. Ohtani and T. Tamao. Does the ballooning instability trigger substorms in the near-earth magnetotail? *Jour. of Geophys. Res.*, 98:19369–19379, 1993.

[19] S. Ortolani and D.D. Schnack. *Magnetohydrodynamics of plasma relaxation*. World Scientific, 1 edition, 1993.

[20] D. Pfirsch and R. N. Sudan. Nonlinear ideal magnetohydrodynamic instabilities. *Phys. Fluids*, 7:2052–2061, 1993.

[21] W.H. Press, S.A. Teukolsky, W.T. Vetterling, and B.P. Flannery. *Numerical Recipes in Fortran*. Cambridge University Press, 2 edition, 1992.

[22] G. J. Rickard and A. N. Wright. Alfven resonance excitation and fast wave propagation in magnetospheric waveguides. *J. Geophys. Res.*, 99:13455–13464, 1994.

[23] G. Rostoker, S.I. Akasofu, J. Foster, R.A. Greenwald, Y. Kamide, K. Kawasaki, A.T.Y. Lui, R.L. McPherron, and C.T. Russell. Magnetic substorms - definitions and signatures. *Jour. of Geophys. Res.*, 85:1663, 1980.

[24] J.C. Samson, D.D. Wallis, T.J. Hughes, F. Creutzberg, J.M. Ruohoniemi, and R.A. Greenwald. Substorm intensification and fieldline resonances in the nightside magnetosphere. *J. Geophys. Res.*, 97:8495–8518, 1992.

[25] B.F. Schutz. *Geometrical Methods of Mathematical Physics*. Cambridge University Press, 1980.

[26] T.H. Stix. *Waves in Plasma*. AIP, 1992.

[27] M. ˘ Svec, T. ˘ Salát, and T. Neubrunn. *Matematická analýza funkcií reálnej premennej*. Alfa SNTL, 1 edition, 1987.

[28] I.O. Voronkov. *Shear Alfven waves and shear flow instabilities in the Earth's magnetosphere*. PhD thesis, University of Alberta, 1998.

[29] I.O. Voronkov, E.F. Donovan, J.C. Samson, L.R. Lyons, and P. Dobias. Near earth breakup in substorms: An empirical and model constraints. *ICS - VI*, 2002.

[30] I.O. Voronkov, R. Rankin, V.T. Tikhonchuk, and J.C. Samson. Nonlinear shear alfven resonances in a dipolar magnetic field. *Jour. of Geophys. Res.*, 102:27137–27143, 1997.

[31] I.O. Voronkov, J.C. Samson, E. Friedrich, R. Rankin, V.T. Tikhonchuk, and E.F. Donovan. On the distinction between, and the relevance of, auroral breakup and substorm expansive phase onset. *ICS - V*, page 249, 2000.

[32] J.A. Wanliss, J.C. Samson, and E. Friedrich. On the use of photometer data to map dynamics of the magnetotail current sheet during substorm growth phase. *Jour. of Geophys. Res.*, 105:27673–27684, 2000.